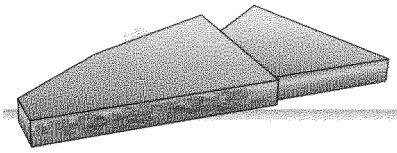

5 CONTAMINANT FATE AND TRANSPORT

Various modeling activities that supported development of this ABRA are discussed below. These activities included source release modeling, dissolved-phase flow and transport modeling, biotic uptake modeling, and VOC transport modeling. Most of the discussion concerns source release and fate and transport modeling for dissolved-phase contaminants. Transport modeling for VOCs was not conducted for this ABRA; however, the results of the VOC transport modeling from the IRA (Becker et al. 1998) were incorporated in the ABRA. Biotic uptake modeling also is presented for the analysis of human health surface exposure pathways and ecological risk assessment.

Modeling in the ABRA is essentially the same as that implemented in the IRA but with some improvements. The differences compared to the IRA models are identified in the discussions below. In general, modeling has three major components: source release, subsurface transport, and transport to the surface. The source release model (DUST-MS [Sullivan 1992]) produces mass estimates used as inputs to the TETRAD subsurface model for fate and transport simulations (Shook 1995) and as inputs to the DOSTOMAN model (Root 1981) to simulate biotic uptake. Numerous model runs were implemented to define a base case analysis and to assess the sensitivity of the results to select model parameters.

All contaminants, except VOCs, were simulated by using the source release model (Disposal Unit Source Term [DUST-MS]), and the biotic uptake model (DOSTOMAN). The results from previous modeling were used to assess VOCs. Because of their low mobility and short half-lives, Cs-137 and Sr-90 were not identified as groundwater pathway risk drivers in the IRA and were eliminated from subsurface modeling. These contaminants were assessed for biotic uptake and surface exposure pathways only. Twenty-nine contaminants were evaluated in the human health analysis, including the 24 human health COPCs identified in the IRA and five additional contaminants that were modeled because they are decay chain members. The long-lived daughter products were specifically included in the simulations because of the possibility of a remedial action slowing transport, which would allow additional ingrowth and influence risk estimates. No extra simulations were performed specifically for the ecological analysis. Biotic modeling used to assess human health risks for surface exposure pathways also provided the basis for ecological risk assessment. Contaminants and models used in the ABRA are summarized in Table 5-1.

5.1 Source Release Modeling

The source term for the ABRA is defined as the waste buried in the SDA. Conceptually, the source term model is simple. Waste was buried in containers such as drums, boxes, and bags. When the containers fail, the contaminants can be released over time by one of three release mechanisms: washoff, diffusion, or dissolution. The type of release mechanism and the release rates are dependent on the characteristics of the waste. The mass released from the buried waste is available for transport to the subsurface by infiltration or to the surface by biotic uptake.

The DUST-MS source release computer code (Sullivan 1992) was used to estimate the mass available for transport. The source term model predicts release of contaminants from the waste buried in the SUA into the subsurface. Version 1.0 of the DUST-MS code (Sullivan 1993) was selected for the WAG 7 RI/FS (Becker 1997). The IRA (Becker et al. 1998) modeled the distributed failure of containers but did not account for releases limited by solubility. The code was enhanced with capability to simulate container failures distributed in time and releases limited by solubility.

Table 5-1. Contaminants evaluated in the Ancillary Basis for Risk Analysis and the computer models used to assess them.

Contaminant	Computer Models			Note
	DUST-MS	TETRAD	DOSTOMAN	
Ac-227	Yes	Yes	Yes	Contaminant of potential concern
Am-241	Yes	Yes	Yes	Contaminant of potential concern
Am-243	Yes	Yes	Yes	Long-lived parent of Pu-239
C-14	Yes	Yes	Yes	Contaminant of potential concern
Cl-36	Yes	Yes	Yes	Contaminant of potential concern
Cs-137	Yes	No	Yes	Contaminant of potential concern for surface exposure pathways only
I-129	Yes	Yes	Yes	Contaminant of potential concern
Nb-94	Yes	Yes	Yes	Contaminant of potential concern
Np-237	Yes	Yes	Yes	Contaminant of potential concern
Pa-231	Yes	Yes	Yes	Contaminant of potential concern
Pb-210	Yes	Yes	Yes	Contaminant of potential concern
PU-238	Yes	Yes	Yes	Long-lived parent of U-234
Pu-239	Yes	Yes	Yes	Contaminant of potential concern
PU-240	Yes	Yes	Yes	Contaminant of potential concern
Ra-226	Yes	Yes	Yes	Contaminant of potential concern
Sr-90	Yes	No	Yes	Contaminant of potential concern for surface exposure pathways only
Tc-99	Yes	Yes	Yes	Contaminant of potential concern
Th-229	Yes	Yes	Yes	Long-lived daughter product of U-233
Th-230	Yes	Yes	Yes	Long-lived daughter product of U-234
Th-232	Yes	Yes	Yes	Long-lived daughter product of U-236
U-233	Yes	Yes	Yes	Contaminant of potential concern
U-234	Yes	Yes	Yes	Contaminant of potential concern
U-235	Yes	Yes	Yes	Contaminant of potential concern
U-236	Yes	Yes	Yes	Contaminant of potential concern
U-238	Yes	Yes	Yes	Contaminant of potential concern
Nitrate	Yes	Yes	Yes	Contaminant of potential concern
Carbon tetrachloride	No	No	No	Contaminant of potential concern-used scaled results from the Interim Risk Assessment (Becker et al. 1998)
Methylene chloride	No	No	No	Contaminant of potential concern-used scaled results from the IRA
Tetrachloroethylene	No	No	No	Contaminant of potential concern-used scaled results from the IRA

Implementation of the source term model is described below. Input parameters include the source term inventory, waste types, infiltration rates, release mechanisms, and release rates. The contaminant grouping and the assignment of SDA contaminants to source areas also are described. The source release model provided mass estimates for total yearly releases from all waste source areas, which were then used as inputs for the subsurface and biotic transport models discussed in the remainder of Section 5.

5.1.1 Source Term Inventory

Annual best-estimate inventories for waste buried in the SDA through 1999 were taken from CIDRA and input into the source term model. Actual disposal quantities were modeled for the base case. Estimates for future disposals in active LLW pits were assessed through sensitivity analyses (see Table 4-1 for the annual disposal inventories for radionuclides and Table 4-2 for nonradionuclides). Total inventories in Tables 4-1 and 4-2 differ from those presented in the IRA for two reasons: (a) the original inventory estimates were modified to reflect the corrections and updates, and (b) this analysis implements best-estimate inventories while the IRA (Becker et al. 1998) considered upper-bound inventories.

Inventories for one COPC (i.e., nitrate) could not be extracted directly from CIDRA because many compounds contain the element nitrogen. Conversion factors used to estimate disposal inventories for nitrate (listed as total nitrogen) are listed in Table 5-2. Conversion factors were taken directly from the MERCK Index (Merck 1989) or developed from the chemical formula and atomic weights of the constituent chemicals. Nitrogen-bearing inventories in CIDRA were multiplied by conversion factors in Table 5-2 to determine the amount of nitrate as total nitrogen buried in the SDA.

Table 5-2. Factors used to convert disposal quantity to amount of contaminant in the total waste stream to nitrate as total nitrogen.

Contaminant	Conversion Factor
Total nitrate (as nitrogen)	—
Aluminum nitrate nonahydrate	0.1972
Ammonia	0.7778
Copper nitrate	0.1489
Mercury nitrate monohydrate	0.0819
Nitric acid	0.2222
Potassium nitrate	0.1386
Sodium nitrate	0.1412
Uranyl nitrate	0.0711

Radioactive decay was the only mechanism considered to affect the source term inventories. As was shown in the IRA, decaying isotopes to the present and then initiating the fate and transport simulations can bias the results low for mobile isotopes with short half-lives. Therefore, inventory estimates for most radionuclides were not adjusted directly to account for radioactive decay. Instead, inventories at the time of disposal were input for each year. The DUST-MS code simulated the inventory changes over time caused by radioactive decay and ingrowth, thus allowing decay and transport to begin at the actual year of disposal.

Inventories for three parent nuclides, Pu-242, Cm-244, and Pu-241, were decayed to the daughter and only the daughters were simulated. In the IRA, risk from Pu-242 was below 1E-12, Cm-244 had a low groundwater risk and is short-lived, and Pu-241 has a short half-life and the risk was 1E-11.

Therefore, all three parent nuclides were decayed to their daughters to minimize the number of isotopes in the subsurface transport simulations.

5.1.2 Container Failure Rates

Distributions to represent failure rates as a function of time for different types of containers such as drums, concrete casks, and metal boxes were developed (Becker et al. 1996; Becker 1997) and implemented in the source term model. Multiple failure rates were assigned to contaminants buried in more than one type of container. For example, if the annual disposal inventory for a particular contaminant included disposals in both drums and cardboard boxes, the relative fraction for each container type was used to model the disposal for that year. For waste streams that were not buried in containers or that were buried in cardboard or wooden boxes, the container failure time in the model was set at zero.

The majority of containers buried in the SDA were 55-gal metal drums. Historical disposal practices included periods when drums were carefully stacked in the SDA and periods when drums were dumped. Drums that were stacked in the SDA provide a barrier to contaminant release until the metal corrodes. Thus, stacked drums fail at a slower rate compared to drums that were dumped into the pits without attempting to maintain their integrity. A separate study was performed to determine the failure rate of metal drums in the SDA using data gathered during earlier waste retrieval efforts (Becker 1997). Failure rate distributions were developed to represent stacked and dumped drums. For stacked drums, a normal distribution with a mean failure time of 22.6 years from the time of disposal and a standard deviation of 9.7 years was developed. For dumped drums the data indicated that 28.5% fail at disposal and that the remaining 71.5% fail in a normal distribution with a mean failure time of 11.7 years from time of disposal and a standard deviation of 5 years. The fraction of a contaminant in drums was modeled with the distributed failure appropriate for the type of drum disposal, whether the drums were stacked or dumped.

The rate of corrosion for carbon steel was used to determine failure time of metal boxes and canisters. Boxes and canisters were considered to fail when one-half of the wall thickness had corroded.

Each waste stream was evaluated for the type of container used. The disposal contents of many waste streams were buried in wood or other readily degradable boxes, and no delay of the contaminant release was assumed for the boxes in the model. Polyethylene bags were not accounted for in the container failure modeling. Calculations by Kudera and Brown (1996) indicated that VOC transport through polyethylene bags is rapid compared to transport through sludge. Therefore, the bags do not limit VOC releases. The 55-gal drums, concrete casks, and metal boxes offer a barrier to contaminant release, which was accounted for in the source term model. Waste streams listed as "O" (i.e., other) in CIDRA, or as a combination of container types without a fractional distribution for each type, were modeled as having no container.

5.1.3 Release Mechanisms and Release Rates

The DUST-MS code is a one-dimensional model that has three contaminant release mechanisms: surface washoff, diffusion, and dissolution. These release mechanisms are described as follows:

- The surface washoff model estimates the release from general laboratory trash and is equivalent to the first-order leach model used in other codes such as GWSCREEN (Rood 1999)

- By applying diffusion coefficients for each waste form, the diffusion model computes the diffusional release from different waste geometries such as VOCs from sludge or cement-encased waste

- The dissolution release model estimates the release caused by general corrosion such as the release of activated metals from the corrosion of the base metal.

Yearly disposal amount of each contaminant was proportioned among the three DUST-MS release mechanisms. The percent of contaminant in a release mechanism was input into the DUST-MS code. Total disposal inventory was analyzed to determine the release mechanism and release rate as a function of the waste stream contents buried in any given year. Table **5-3** contains summary information on the waste streams for each individual contaminant, a brief description of the waste streams, and the release mechanisms identified for use in the modeling of the waste streams.

Because each contaminant has a unique set of information, the disposal amount each year for each contaminant was modeled as a separate waste container. The DUST-MS code was used to compute the sum of the results to provide the total release over the time interval for input into the transport models. A summary of release rate information for the different release models is contained in Table **5-4.** The basis for using the individual values is discussed in the following paragraphs.

Waste streams that are primarily metal were modeled either as dissolution release by corrosion of the base metal or as surface washoff of contamination on the metal. For actinides and fission products, metal waste streams were modeled as surface washoff release of contaminants on the base metal. Activation products are integral to the base metal and are released by dissolution as the metal corrodes. Table **5-5** lists the release mechanism for contaminants in metal waste streams.

Concrete casks were not modeled with an assumed failure time. Instead, release of contaminant mass from within the casks was modeled as diffusion out of the cask. Casks were modeled as cylinders with a 15-cm (6-in.) wall thickness. Using this thickness assumption allows the ready release of contamination at the surface of the cask. In addition, a diffusion coefficient of 1.0E-06 cm^2/s was used. A diffusion coefficient of 1.0E–06 cm^2/s is typical for a metal ion in water and does not account for the possible partitioning of the contaminant with the waste form or the porous media that the contaminants must travel through. Any partitioning would slow the contaminant release.

Nagata and Banaee (1996) assessed the metals buried in the SDA and concluded that the majority is a form of stainless steel or inconel (nickel-based alloy). Nagata and Banaee (1996) provided a corrosion rate of 1 mm in 4,500 years (2.22E-05 cm/year) for stainless steel in INEEL soil with a magnesium chloride dust suppressant applied. For beryllium the corrosion rate is based on results of a long-term corrosion and degradation test, Adler Flitton et al. **(2001).** The measured results from the test were modified to include the effect of the magnesium chloride dust suppressant that was applied to the surface of the SDA. The chloride in the dust suppressant would increase the corrosion rate of the beryllium metal. The beryllium corrosion rate is different from that used in the IRA.

Table 5-3. Waste streams for Waste Area Group 7 contaminants of potential concern and long-lived decay chain members.

Contaminant	Waste Stream Code or Waste Generator	Percent of Total in Waste Stream	Total Inventory (Ci)	Waste Stream Description	Release Mechanism
Ac-227	D&D-ARA-1	3.6	1.82E-08	Low-level waste (LLW) from decontamination and demolition of the Auxiliary Reactor Area (ARA) (primarily contaminated metal and debris)	Surface washoff
	CFA-RWM-1	14.1	7.20E-08	Central Facilities Area (CFA) Sewage Treatment Plant unpainted concrete rubble, drying beds soils, clarifier piping, and trickle filter bricks	Surface washoff
	Test Reactor Area	34.3	1.76E-07	Beryllium blocks	Dissolution
	CFA-690-1	47.5	2.43E-07	Combustibles, animal carcasses, scrap metal, sources, sand, and gravel	Surface washoff
	Miscellaneous	0.6	2.86E-09	Miscellaneous minor streams	Surface washoff
Total Ac-227		**100.0**	**5.12E-07**		
Am-243	Idaho National Engineering and Environmental Laboratory (INEEL)	99.6	1.34E+02	Idaho National Engineering and Environmental Laboratory (INEEL) reactor operations waste	Surface washoff
	Miscellaneous	0.4	- 0	Miscellaneous minor streams	Surface washoff
Total Am-243		**100.0**	**1.34E+02**		
Am-241	INEEL	2.2	4.01E+03	INEEL reactor operations waste	Surface washoff
	RFO-DOW-12H	2.6	4.85E+03	Dirt, concrete, graphite, ash, and soot	Surface washoff
	RFO-DOW-4H	13.8	2.52E+04	Combustibles: paper, rags, plastic clothing cardboard, wood, and polyethylene bottles (Codes 330,336,337,900, and 970)	Surface washoff
	RFO-DOW-3H	80.0	1.46E+05	Uncemented sludge	Surface washoff

Table 5-3. (continued).

Contaminant	Waste Stream Code or Waste Generator	Percent of Total in Waste Stream	Total Inventory (Ci)	Waste Stream Description	Release Mechanism
	Miscellaneous	1.4	2.56E+03	Miscellaneous minor streams	Surface washoff
Total Am-241		**100.0**	**1.83E+05**		
C-14	ANL-785-1	1.5	7.51E+00	Subassembly LLW from Hot Fuel Examination Facility experiments	Dissolution
	TRA-603-1H	1.6	7.81E+00	Test Reactor Area (TRA) resins	Surface washoff
	Argonne National Laboratory – West (ANL-W)	3.3	1.66E+01	Subassembly hardware	Dissolution
	CPP-603-1H	9.2	4.58E+01	Fuel end pieces	Dissolution
	TRA	18.5	9.26E+01	Beryllium waste	Dissolution
	NRF-616-3H, 4H, 8H	21.3	1.07E+02	Core structural pieces	Dissolution
	TRA	41.7	2.08E+02	Activation products	Dissolution
	Miscellaneous	2.9	1.45E+01	Miscellaneous minor streams	Surface washoff
Total C-14		**100.0**	**5.00E+02**		
C1-36	NRF-618-8R	9.1	1.01E-01	Structural components from reactor fuel modules (e.g., end boxes) from 1989 to 1993	Surface washoff
	OFF-UBM-1H	31.0	3.43E-01	Ore processing waste	Surface washoff
	TRA	59.9	6.62E-01	Beryllium blocks	Dissolution
Total Cl-36		**100.0**	**1.11E+00**		
Cs-137	INEEL	21.4	1.32E+05	INEEL reactor operations	Surface washoff
	TRA-603-15H	16.9	1.04E+05	Metal	Surface washoff
	ANL-765-2H	14.5	8.94E+04	Subassembly hardware	Surface washoff
	TRA-642-6H	9.8	6.02E+04	Scrap metal	Surface washoff
	TRA-603-1H	7.9	4.86E+04	Resins	Surface washoff

Table 5-3. (continued).

Contaminant	Waste Stream Code or Waste Generator	Percent of Total in Waste Stream	Total Inventory (Ci)	Waste Stream Description	Release Mechanism
	ANL-785-1H	6.9	4.23E+04	Subassembly hardware	Surface washoff
	TRA-603-4H	4.3	2.64E+04	Core and loop components	Surface washoff
	OFF-ATI-1H	4.2	2.56E+04	Fuel	Surface washoff
	TRA-603-9H	3.5	2.20E+04	Fuel	Surface washoff
	ANL-765-1H	1.8	1.10E+04	Dry active waste	Surface washoff
	CPP-633-1H	1.3	7.76E+03	High-efficiency particulate air filters	Surface washoff
	Miscellaneous	7.7	4.75E+04	Miscellaneous minor streams	Surface washoff
Total Cs-137		**100.0**	**6.17E+05**		
I-129	PBF-620-1	1.2	1.90E-03	Miscellaneous scrap	Surface washoff
	Naval Reactors Facility	1.7	2.67E-03	Test specimens	Surface washoff
	INEEL	94.5	1.49E-01	INEEL reactor operations waste	Surface washoff
Total 1-129		**100.0**	**1.58E-01**		
Nb-94	TRA	4.0	4.06E+01	Activation products	Dissolution
	CPP-603-1H	4.7	4.74E+01	Fuel end pieces	Dissolution
	NRF-618-12H	1.3	1.31E+01	Core structural components	Dissolution
	INEEL	87.6	8.80E+02	INEEL reactor operations waste	Dissolution
	Miscellaneous	2.3	2.31E+01	Miscellaneous minor streams	Surface washoff
Total Nb-94		**100.0**	**1.00E+03**		
Np-237	TRA-632-1H	1.3	3.42E-02	Core structural pieces	Surface washoff
	TRA-603-9H	4.6	1.22E-01	Expended fuel and ceramic fuel	Surface washoff
	TRA-603-4H	6.6	1.74E-01	Core and loop components	Surface washoff
	TRA-642-6H	15.0	3.96E-01	Core, vessel, and loop components	Surface washoff
	TRA-603-1H	15.6	4.13E-01	Resins	Surface washoff

Table 5-3. (continued).

Contaminant	Waste Stream Code or Waste Generator	Percent of Total in Waste Stream	Total Inventory (Ci)	Waste Stream Description	Release Mechanism
	TRA-603-15H	25.9	6.85E-01	Metal	Surface washoff
	INEEL	28.5	7.54E-01	INEEL reactor operations waste	Surface washoff
	Miscellaneous	2.5	6.61E-02	Miscellaneous minor streams	Surface washoff
Total Np-237		**100.0**	**2.64 E+00**		
Pa-231	D&D-ARA-1	99.0	8.56E-04	The LLW from the decontamination and demolition of the ARA facilities (primarily of contaminated metal and debris)	Surface washoff
	Miscellaneous	1.0	8.44E-06	Miscellaneous minor streams	Surface washoff
Total Pa-231		**100.0**	**8.64E-04**		
Pb-210	WER-CMP-1	5.3	2.70E-08	Compacted waste: combination of glass, plastic, absorbents, cloth, paper, and wood	Surface washoff
	ALE-ALE-1H	94.7	4.83E-07	Building rubble, electric wires, piping, machinery, tracers and sources, glass, gloves, paper, filters, and vermiculite	Surface washoff
Total Pb-210		**100.0**	**5.10E-07**		
Pu-240	RFO-DOW-5H	1.7	2.82E+02	Concrete and brick	Surface washoff
	OFF-LRL-2H	2.7	4.53E+02	Concrete, bricks, and asphalt	Surface washoff
	RFO-DOW-11H	4.5	7.62E+02	Graphite molds	Surface washoff
	RFO-DOW-8H	6.0	1.02E+03	Lead from glovebox gloves and sheeting	
	RFO-DOW-7H	7.1	1.21E+03	Glass, including raschig rings	Surface washoff
	RFO-DOW-4H	7.9	1.35E+03	Combustibles: paper, rags, plastic clothing cardboard, wood, and polyethylene bottles (Codes 330, 336, 337, 900, and 970)	Surface washoff
	RFO-DOW-12H	9.0	1.53E+03	Dirt, concrete, graphite, ash, and soot	Surface washoff
	RFO-DOW-6H	10.4	1.78E+03	Filters	Surface washoff
	RFO-DOW-3H	12.4	2.12E+03	Uncemented sludge	Surface washoff

Table 5-3. (continued).

Contaminant	Waste Stream Code or Waste Generator	Percent of Total in Waste Stream	Total Inventory (Ci)	Waste Stream Description	Release Mechanism
	INEEL	13.8	2.36E+03	INEEL reactor operations waste	Surface washoff
	RFO-DOW-9H	22.5	3.85E+03	Noncombustibles: gloveboxes, equipment, pumps, motors, control panels, and office equipment	Surface washoff
	Miscellaneous	2.0	3.42E+02	Miscellaneous minor streams	Surface washoff
Total Pu-240		**100.0**	**1.71E+04**		
Pu-239	RFO-DOW-13H	1.1	7.31E+02	Resins	Surface washoff
	RFO-DOW-5H	1.9	1.25E+03	Concrete and brick	Surface washoff
	INEEL	2.0	1.29E+03	INEEL reactor operations waste	Surface washoff
	RFO-DOW-11H	5.2	3.37E+03	Graphite molds	Surface washoff
	RFO-DOW-8H	7.0	4.53E+03	Lead from glovebox gloves and sheeting	Surface washoff
	RFO-DOW-7H	8.3	5.37E+03	Glass: including raschig rings	Surface washoff
	RFO-DOW-4H	9.2	5.96E+03	Combustibles: paper, rags, plastic clothing cardboard, wood, and polyethylene bottles (Codes 330,336,337,900, and 970)	Surface washoff
	RFO-DOW-12H	10.5	6.79E+03	Dirt, concrete, graphite, ash, and soot	Surface washoff
	RFO-DOW-6H	12.2	7.90E+03	Filters	Surface washoff
	RFO-DOW-3H	14.5	9.40E+03	Uncemented sludge	Surface washoff
	RFO-DOW-9H	26.3	1.70E+04	Noncombustibles: gloveboxes, equipment, pumps, motors, control panels, and office equipment	Surface washoff
	Miscellaneous	1.9	1.23E+03	Miscellaneous minor streams	Surface washoff
Total Pu-239			**6.49E+04**		
Pu-238	RFO-DOW-4H	10	1.74E+02	Combustibles: paper, rags, plastic clothing cardboard, wood, and polyethylene bottles (Codes 330,336,337,900, and 970)	Surface washoff

Table 5-3. (continued).

Contaminant	Waste Stream Code or Waste Generator	Percent of Total in Waste Stream	Total Inventory (Ci)	Waste Stream Description	Release Mechanism
	RFO-DOW-12H	1.2	1.99E+02	Dirt, concrete, graphite, ash, and soot	Surface washoff
	RFO-DOW-6H	1.4	2.32E+02	Filters	Surface washoff
	RFO-DOW-3H	1.6	2.75E+02	Uncemented sludge	Surface washoff
	TRA-603-9H	2.9	4.95E+02	Expended fuel and ceramic fuel	Surface washoff
	RFO-DOW-9H	2.9	5.00E+02	Noncombustibles: gloveboxes, equipment, pumps, motors, control panels, and office equipment	Surface washoff
	INEEL	85.3	1.46E+04	INEEL reactor operations waste	Surface washoff
	Miscellaneous	3.8	6.50E+02	Miscellaneous minor streams	Surface washoff
Total Pu-238		**100.0**	**1.71E+04**		
Ra-226	ALE-ALE-1H	1.7	9.93E-01	Building rubble, electric wires, piping, machinery, tracers and sources, glass, gloves, paper, filters, and vermiculite	Surface washoff
	TAN-640-1H	1.7	1.00E+00	Radium-beryllium neutron source	Surface washoff
	ALE-317-2R	1.8	1.10E+00	Combustibles	Surface washoff
	TRA-603-22H	2.1	1.25E+00	Combustibles	Surface washoff
	TRA-603-8H	2.1	1.25E+00	Two Ra-226 sources	Surface washoff
	OFF-DPG-1H	2.8	1.67E+00	Biological waste	Surface washoff
	OFF-AEF-1H	5.6	3.33E+00	Wipes, gloves, glassware, and dry activated waste embedded in concrete	Surface washoff
	OFF-ISC-1H	8.3	5.00E+00	Magnesium-thorium scrap, sources, and miscellaneous laboratory equipment	Surface washoff
	OFF-USN-1H	72.3	4.33E+01	Animal carcasses, waste-paper towels, glassware, tools, and laboratory items	Surface washoff
	Miscellaneous	1.7	1.02E+00	Miscellaneous minor streams	Surface washoff
Total Ra-226		**100.0**	**6.00E+01**		

Table 5-3. (continued).

Contaminant	Waste Stream Code or Waste Generator	Percent of Total in Waste Stream	Total Inventory (Ci)	Waste Stream Description	Release Mechanism
Sr-90	INEEL	60.3	3.89E+05	INEEL reactor operations waste	Dissolution
	ANL-765-2H	21.6	1.39E+05	Subassembly hardware	Dissolution
	ANL-785-1H	10.1	6.60E+04	Subassembly hardware	Dissolution
	ANL-765-1H	2.3	1.48E+04	Dry active waste	Dissolution
	CPP-601-1H	1.5	9.85E+03	Leached Vycor glass	Surface washoff
	CPP-601-3H	1.0	4.00E+03	Dissolved fuel specimens	Surface washoff
	Miscellaneous	3.4	2.19E+04	Miscellaneous minor streams	Surface washoff
Total Sr-90		**100.0**	**6.44E+05**		
Tc-99	D&D-ARA-1	1.1	6.42E-01	LLW from the decontamination and demolition of the ARA facilities (primarily contaminated.	Surface washoff
	NRF	2.6	1.56E+00	Test specimens	Surface washoff
	ANL metal	2.9	1.75E+00	Subassembly hardware	Surface washoff
	INEEL	89.9	5.44E+01	INEEL reactor operations waste	Surface washoff
	Miscellaneous	3.5	2.12E+00	Miscellaneous minor streams	Surface washoff
Total Tc-99		**100.0**	**6.05E+01**		
Th-232	TAN-607-2	1.1	1.41E-02	Test Area North (TAN) Hot Shop noncompactable waste	Surface washoff
	OFF-GDA-1H	1.5	2.00E-02	Fuel fabrication item, laboratory equipment, activated metal, and irradiated fuel	Surface washoff
	TRA-603-9H	1.5	2.01E-02	Expended fuel and ceramic fuel	Surface washoff
	OFF-UBM-1H	93.5	1.26E+00	Ore processing waste	Surface washoff
	Miscellaneous	2.5	3.36E-02	Miscellaneous minor streams	Surface washoff
Total Th-232		**100.0**	**1.34E+00**		

Table 5-3. (continued).

Contaminant	Waste Stream Code or Waste Generator	Percent of Total in Waste Stream	Total Inventory (Ci)	Waste Stream Description	Release Mechanism
Th-230	TAN-607-2	7.5	2.34E-03	TAN Hot Shop noncompactable waste	Surface washoff
	D&D-ARA-1	34.8	1.09E-02	The LLW from the decontamination and demolition of the ARA facilities (primarily of contaminated metal and debris)	Surface washoff
	WMC-WMC-1H	57.1	1.79E-02	Soil, pond sediment, scrap metal, and equipment	Surface washoff
Total Th-230		**100.0**	**3.13E-02**		
Th-229	TRA	3.9	2.69E-07	Beryllium blocks	Surface washoff
	WER-CMP-1	37.1	2.52E-06	Compacted waste: combination of glass, plastic, absorbents, cloth, paper, and wood	Surface washoff
	CPP-ALL-1	58.8	4.01E-06	Contaminated structural materials (metal, concrete, bricks, soil, gravel, wood, and plastics) and concreted ash processed at the Waste Experimental Reduction Facility	Surface washoff
	Miscellaneous	0.1	6.81E-06	Miscellaneous minor streams	Surface washoff
Total Th-229		**100.0**	**6.81E-06**		
U-233	SMC-628-1	1.5	2.21E-02	Nonacidic evaporator sludge	Surface washoff
	SMC-990-1	1.8	2.74E-02	Depleted uranium-contaminated material (metals, glass, and gravel)	Surface washoff
	SMC-628-2	19.9	3.01E-01	Unsolidified slag	Surface washoff
	RFO-DOW-19H	35.9	5.40E-01	Miscellaneous scrap	Surface washoff
	ARA-626-1H	39.8	6.00E-01	Fuel scrap, waste from disassembly of facilities and hot cell waste	Surface washoff
	Miscellaneous	1.1	1.66E-02	Miscellaneous minor streams	Surface washoff
Total U-233		**100.0**	**1.51E+00**		
U-234	ALE-317-2R	1.1	7.10E-01	Combustibles	Surface washoff
	TRA-603-15H	1.6	1.11E+00	Metal	Surface washoff

Table 5-3. (continued).

Contaminant	Waste Stream Code or Waste Generator	Percent of Total in Waste Stream	Total Inventory (Ci)	Waste Stream Description	Release Mechanism
	ANL-704-1R	1.8	1.21E+00	Contact-handled fuel fabrication waste	Surface washoff
	OFF-CSM-1H	1.9	1.30E+00	Magnesium fluoride slag and miscellaneous laboratory waste	Surface washoff
	ANL-752-1R	2.0	1.33E+00	Contact-handled waste	Surface washoff
	TAN-607-2	2.7	1.83E+00	TAN Hot Shop noncompactable waste	Surface washoff
	OFF-GEC-1H	4.4	2.95E+00	Core, vessel, and loop components	Surface washoff
	ANL-EBRI-1H	5.0	3.36E+00	Miscellaneous combustibles and core, vessel, and loop components	Surface washoff
	OFF-ATI-1H	5.4	3.64E+00	Irradiated fuel from research	Surface washoff
	PDA-RFO-1A	6.9	4.64E+00	Inorganic salts, depleted uranium, and sewage sludge	Surface washoff
	CPP-601-3H	7.0	4.70E+00	Dissolved fuel specimens	Surface washoff
	RFO-DOW-16H	21.5	1.45E+01	Depleted uranium	Surface washoff
	RFO-DOW-18H	31.9	2.15E+01	Enriched uranium	Surface washoff
	Miscellaneous	6.9	4.65E+00	Miscellaneous minor streams	Surface washoff
Total U-234		**100.0**	**6.74E+01**		
U-235	ANL-752-1R	1.0	5.60E-02	Contact-handled waste	Surface washoff
	OFF-GDA-1H	1.3	7.00E-02	Fuel fabrication item, laboratory equipment, activated metal, and irradiated fuel	Surface washoff
	OFF-CSM-1H	1.4	8.00E-02	Magnesium fluoride slag and miscellaneous laboratory waste	Surface washoff
	ANL-EBRI-1H	2.0	1.10E-01	Miscellaneous combustibles and core, vessel, and loop components	Surface washoff
	OFF-ATI-1H	2.1	1.14E-01	Irradiated fuel from research	Surface washoff
	INEEL	2.3	1.28E-01	INEEL reactor operations waste	Surface washoff
	CPP-601-3H	2.7	1.50E-01	Dissolved fuel specimens	Surface washoff

Table 5-3. (continued).

Contaminant	Waste Stream Code or Waste Generator	Percent of Total in Waste Stream	Total Inventory (Ci)	Waste Stream Description	Release Mechanism
	OFF-GEC-1H	2.8	1.57E-01	Core, vessel, and loop components	Surface washoff
	WAG-WG7-02	3.3	1.80E-01	Acid Pit in situ stabilization treatability study	Surface washoff
	PDA-RFO-1A	5.9	3.25E-01	Inorganic salts, depleted uranium, and sewage sludge	Surface washoff
	TRA-603-6H	7.3	4.02E-01	Core, vessel, and loop components	Surface washoff
	TRA-603-15H	9.7	5.35E-01	Metal	Surface washoff
	RFO-DOW-18H	13.4	7.44E-01	Enriched uranium	Surface washoff
	TRA-603-16H	14.1	7.80E-01	Combustibles	Surface washoff
	RFO-DOW-16H	19.5	1.08E+00	Depleted uranium	Surface washoff
	Miscellaneous	11.3	6.26E-01	Miscellaneous minor streams	Surface washoff
Total U-235		**100.0**	**5.54E+00**		
U-236	SMC-628-2	1.5	4.37E-02	Unsolidified slag	Surface washoff
	NRF	1.8	5.29E-02	Test specimens	Surface washoff
	RFO-DOW-18H	2.8	8.04E-02	Enriched uranium	Surface washoff
	TRA-603-9H	2.8	8.11E-02	Expended fuel and ceramic fuel	Surface washoff
	TRA-603-4H	3.7	1.07E-01	Core and loop components	Surface washoff
	TRA-642-6H	8.5	2.44E-01	Core, vessel, and loop components	Surface washoff
	TRA-603-1H	9.4	2.70E-01	Resins	Surface washoff
	TRA-603-15H	14.7	4.22E-01	Metal	Surface washoff
	INEEL	20.4	5.83E-01	INEEL reactor operations waste	Surface washoff
	RFO-DOW-16H	31.5	9.03E-01	Depleted uranium	Surface washoff
	Miscellaneous	2.6	7.44E-02	Miscellaneous minor streams	Surface washoff
Total U-236		**100.0**	**2.86E+00**		

Table 5-3. (continued).

Contaminant	Waste Stream Code or Waste Generator	Percent of Total in Waste Stream	Total Inventory (Ci)	Waste Stream Description	Release Mechanism
U-238	INEEL	1.1	1.30E+00	INEEL reactor operations waste	Surface washoff
	ALE-ALE-1H	1.1	1.32E+00	Building rubble, electric wires, piping, machinery, tracers and sources, glass, gloves, paper, filters, and vermiculite	Surface washoff
	OFF-CSM-1H	1.1	1.32E+00	Magnesium fluoride slag and miscellaneous laboratory waste	Surface washoff
	ARA-627-1H	1.4	1.64E+00	Fuel scrap, waste from disassembly of facilities, and hot cell waste	Surface washoff
	SMC-628-2	2.0	2.31E+00	Unsolidified slag	Surface washoff
	PDA-RFO-1A	21.2	2.49E+01	Inorganic salts, depleted uranium, and sewage sludge	Surface washoff
	RFO-DOW-16H	65.0	7.62E+01	Depleted uranium	Surface washoff
	Miscellaneous	7.0	8.20E+00	Miscellaneous minor streams	Surface washoff
Total U-238		**100.0**	**1.17E+02**		
Nitrate	CPP-601-4H	11.0	1.13E+08	Acidic aqueous liquid	Surface washoff
	PDA-RFO-1A	53.0	5.46E+08	Nitrate salts Rocky Flats Plant (RFP) sludge	Surface washoff
	RFO-DOW-17H	36.0	3.71E+08	Nitrate salts in sludge	Surface washoff
Total Nitrate (as nitrogen)		**100.0**	**1.03E+09**		
Carbon tetrachloride	RFO-DOW-4H	2.5	2.05E+07	Paper, rags, and plastic	Vapor diffusion
	RFO-DOW-15H	96.8	7.94E+08	Organic sludge	Vapor diffusion
	Miscellaneous	0.7	5.74E+06	Miscellaneous minor streams	Vapor diffusion
Total carbon tetrachloride		**100**	**8.20E+08**		

Table 5-3. (continued).

Contaminant	Waste Stream Code or Waste Generator	Percent of Total in Waste Stream	Total Inventory (Ci)	Waste Stream Description	Release Mechanism
Methylene chloride	RFO-DOW-12H	9.3	1.30E+06	Dirt, sand, concrete, ashes, and soot	Vapor diffusion
	RFO-DOW-9H	18.3	2.56E+06	Equipment (drill presses, lathes, and pumps)	Vapor diffusion
	RFO-DOW-4H	20.3	2.84E+06	Paper, rags, and plastic	Vapor diffusion
	RFO-DOW-3H	51.2	7.16E+06	Uncemented sludge	Vapor diffusion
	Miscellaneous	1.0	1.40E+05	Miscellaneous minor streams	Vapor diffusion
Total methylene chloride		**100.0**	**1.40E+07**		
Tetrachloroethylene	RFO-DOW-15H	100.0	9.80E+07	Organic sludge	Vapor diffusion
Total tetrachloroethylene		**100.0**	**9.8E+07**		

Table 5-4. Summary of release types and release rate coefficients applied in the source release modeling.

Release Type	Release Rate Coefficient	Reference
Container failure rate	Site-specific values	See Section 5.1.2
Corrosion of carbon steel	1 mm in 450 to 680 years	Nagata and Banaee (1996)
Corrosion of stainless steel	1 mm in 4,500 years (1.19E-05/year)	Adler Flitton et al. (2001)
Beryllium corrosion	1 mm in 39.37 years (2.65E-03/year)	Adler Flitton et al. (2001)
Metal corrosion	Contaminant solubility	Dicke (1997) (see Section 5.2)
Resin dissolution	Surface washoff model was used	Dicke (1997) (see Section 5.2)
Surface washoff	Soil-to-water partition coefficients	Dicke (1997) (see Section 5.2)
Volatile organic compound diffusion	2E-03 cm^2/second (soil) to 5E-09 cm^2/second (saturated saltstone) 1.5E-08 cm^2/second is recommended	Kudera and Brown (1996)

Table 5-5. Waste stream release mechanisms for actinides, activation products, and fission products.

Type of Contaminant	Release Mechanism	Contaminants
Actinides	Surface washoff	Am-241, Am-243, Np-237, Pu-238, Pu-239, Pu-240, U-233, U-234, U-235, U-236, and U-238
Activation products	Dissolution	C-14, Nb-94, and Tc-99
Fission products	Surface washoff	Cs-137, I-129, and Sr-90

Geometry used for the steel pieces also was modified from the IRA. Review of available data showed the surface-area-to-volume ratio for typical INEEL-type reactors to be 0.535/cm (Oztunali and Roles 1985). Combining the corrosion rate and geometry data provided a fractional release from stainless steel of 1.19E-05/year. Similarly, the corrosion rate of beryllium blocks was based on the long-term corrosion and degradation test (Adler Flitton et al. 2001). As for stainless steel, measured beryllium corrosion was modified to account for chloride in the dust suppressant. The corrosion rate of the beryllium blocks used was 1 mm in 39.37 years (2.54E-03 cm/year). The surface-area-to-volume ratio of the beryllium blocks is 1.043/cm. Combining geometry data with the corrosion rate provides a fractional release from the beryllium blocks of 2.65E-03/year.

The above discussion applies to integral contamination of steels. Release of other metals (e.g., lead) into the subsurface is dependent on chemical properties of soil water and solubility of that metal in INEEL pore water conditions. Soil water has a high pH, causing many contaminants to have a low solubility (Dicke 1997). To simulate release of metals (e.g., lead), the surface washoff release model was used with the appropriate contaminant-specific solubility limit for INEEL soil water chemistry.

Sludge buried at the SDA contains VOCs, radioactive contaminants, and other hazardous constituents. Release of VOCs from sludge is through vapor diffusion (Kudera and Brown 1996). As shown in Table 5-4, release rates can vary by several orders of magnitude. The value used in the IRA

(Becker et al. 1998) was 2E-06 cm^2/second. Release of metals and radioactive contaminants from sludge occurs through leaching, which was modeled with the surface washoff release model.

A surface washoff release mechanism was assumed for waste streams that are generic laboratory trash. The surface washoff release mechanism provides the most rapid release rates. Similarly, contaminants identified as surface contamination of a base material (e.g., anticontamination clothing) were modeled with the surface washoff release model. The surface washoff model applies a partition coefficient to determine the release. The soil-to-water partition coefficient was used as a first approximation.

The surface washoff release model was used to simulate the release from resins. For activation and fission products, using surface washoff release generates a higher release rate, which is appropriate because these contaminants are generally mobile (low K_d). Resin would sorb the contaminant better than soil.

5.1.4 Contaminant Grouping for Modeling

Release and subsurface transport were simulated for 24 contaminants, which were grouped into seven groups of contaminants for fate and transport simulation. This grouping was used in source term simulations to provide a consistent set of inputs for the biotic uptake model (DOSTOMAN) and the subsurface model (TETRAD). Members of a decay chain are assigned to the same group. Isotopes in the chain with a half-life of more than 1 year were included explicitly in the simulations, while contaminants with shorter half-lives were assumed to be in equilibrium with long-lived parents. Grouping for the COPCs and long-lived decay chain members is defined in Table 5-6 as Groups 1 through 5. Some of the long-lived daughter products were not identified as COPCs in the IRA (Becker et al. 1998) but were included here to confirm that they pose no unacceptable risk and to assess sensitivity and uncertainty. Some of the ABRA sensitivity cases reduce the release of the parent nuclide and thus increase the ingrowth of the daughter in the waste zone.

Table 5-6. Contaminant grouping for simulations implemented for the Pre-Draft Remedial Investigation/Baseline Risk Assessment.

Simulation Group	Contaminants in the Group	Description	Basis[a]
Group 1	Am-241, Np-237, U-233, and Th-229	Pu-241 decay chain	Neptunium series beginning at Pu-241 created by nuclear reactions.
Group 2	Pu-239, U-235, Pa-231, Ac-227, and Am-243	Am-243 and Pu-239 decay chain	Am-243 to Pu-239, both created by nuclear reactions, to actinium series initiated by U-235.
Group 3	Pu-240, U-236, and Th-232	Pu-240 decay chain	Pu-240 to U-236 created by nuclear reactions to thorium series initiated by Th-232.
Group 4	Pu-238, U-234, Th-230, Ra-226, and Pb-210	Pu-238 decay chain	Pu-238 created by nuclear reactions to U-234 to mid-uranium series.
Group 5	U-238, U-234, Th-230, Ra-226, and Pb-210	U-238 decay chain	Uranium series initiated by U-238.
Group 6	Nitrate	Toxic chemicals	Contained primarily in Rocky Flats Plant waste.
Group 7	Tc-99, I-129, C-14, Nb-94. and C1-36	Fission and activation products	Created by nuclear reactions.

a. Shleien (1992).

5.1.5 Simulated Source Areas

In the ABRA modeling, distribution of waste in the SDA was substantially refined relative to the IRA. At the time of the IRA, data were insufficient to proportion waste into individual pits or trenches; however, information on the shipping records was subsequently input into WasteOScope database (INEEL 2002a, 2002b). Use of WasteOScope has facilitated modeling of the distribution of the contaminant mass to specific source areas in the SDA based on actual disposal records. The SDA was divided into 13 source areas for modeling contaminant release and transport. These source areas are listed in Table 5-7, which also includes a brief description of the disposals composing them. Each source area is represented in the subsurface model grid as illustrated in Figure 5-1. Note that the pits are individually modeled (except for Pits 1 and 2, which are adjoining), whereas the trenches and soil vaults are modeled together. Because DUST-MS is a one-dimensional model, multiple simulations were implemented for each contaminant group to simulate the release from each source area individually. Results were then combined for input into the subsurface transport and biotic uptake simulations.

Table 5-7. Source areas in the Subsurface Disposal Area implemented in the source release model.

Source Area	Description[a]	Area (ft^2)	Open	Closed
1	Trenches 1–10	120,960	July 8, 1952	February 7, 1958
2	Pits 1 and 2	103,338	November 1, 1957	July 1, 1963
3	Pit 3	41,830	December 15, 1961	January 3,1963
4	Pit 4	111,732	January 3,1963	September 26, 1967
5	Pit 5	108,754	June 18,1963	December 22, 1966
6	Pit 6	54,984	May 18,1967	October 22, 1968
7	Pit 8	31,294	March 6, 1967	November 30,1969
8	Pit 9	45,541	November 8, 1967	June 9, 1969
9	Pit 10	111,732	June 7,1968	July 8, 1971
10	Pad A[b]	32,160	September 26, 1972	November 17, 1978
11	Low-level waste Pits 17 through 20[c,d]	97,051	June 25,1975	December 31, 1999[e]
12	Projected low-level waste Pits 17 through 20	36,000	January 1,2000	Projected to 2010[e]
13	All soil vault rows[c]	2,849	March 2,1977	April 15, 1995

a. Pit 7 had only five disposals and was not assigned to a source area. The acid pit was not assigned to a source area because it contains no contaminants of potential concern and was eliminated from further evaluation (DOE-ID 1998).

b. Pad A waste includes part of the waste that was originally disposed of in Pits 11 and 12. Residual inventory in Pits 11 and 12 were assigned to the Pad A source area.

c. Trenches 11 through 58 were not explicitly modeled. The inventories in Trenches 11 through 58 were partitioned between the soil vaults and the active low-level waste (LLW) pit, depending on the waste stream.

d. Pits 13 through 16 received LLW from on-Site generators and the inventories were assigned to the LLW pit.

e. The LLW disposal operation is still active. Actual disposals in Pits 17 through 20 were implemented in the model for Source Area 11. Projected disposals were evaluated in Source Area 12.

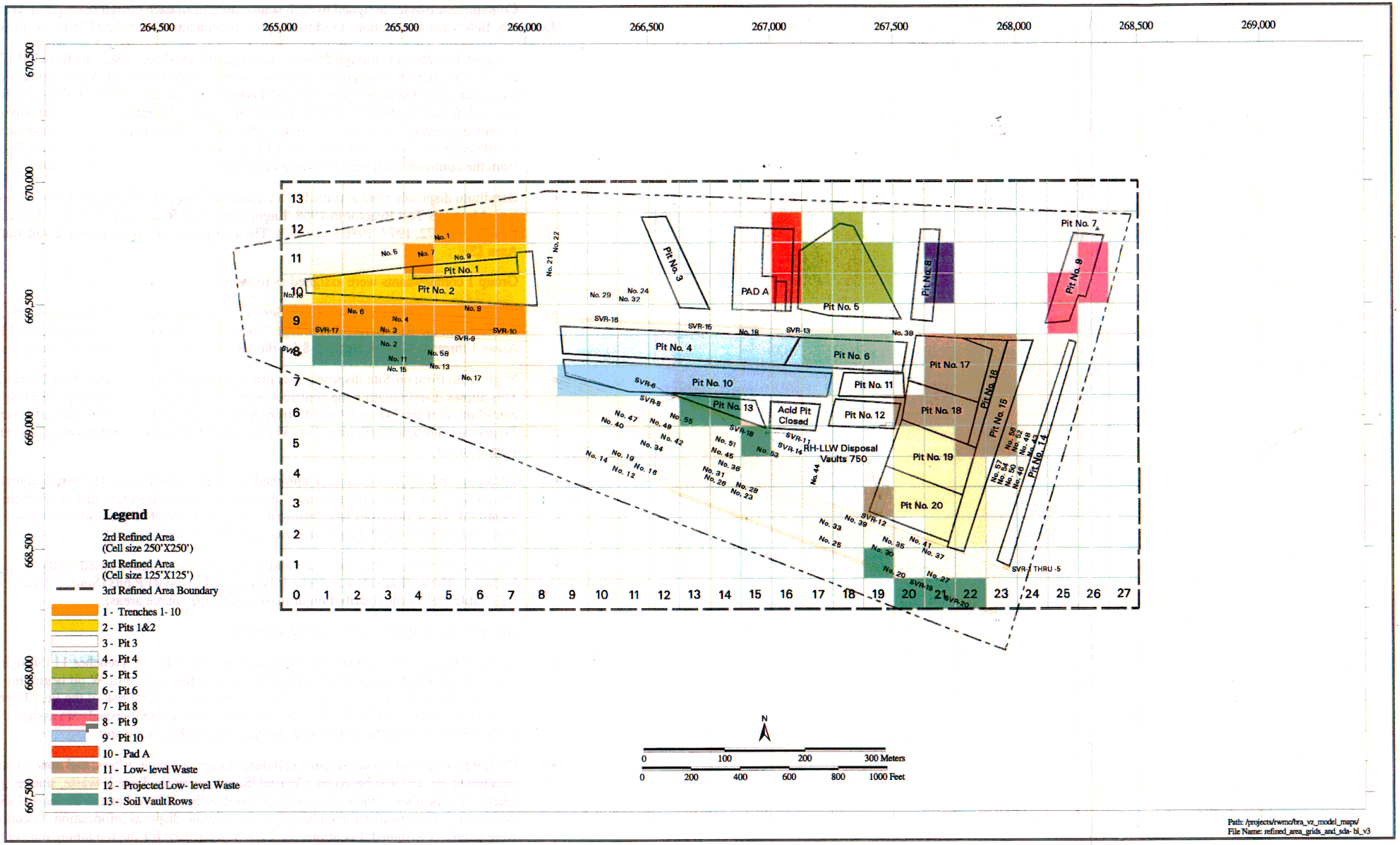

Figure 5-1. The 13 areas simulated in the source release model and specifically represented in the subsurface model domain.

Contaminant masses assigned to each source area from each contaminant group are given in Table 5-8. Below are assumptions used to assign contaminants within the SDA to the 13 source areas.

- Because Trenches 11 through 58 were not explicitly modeled, disposals from INEEL waste generators (other than beryllium disposals) were modeled in the LLW pit (Source Area 11). A significant contribution to total disposal quantities for Ac-227, Am-243, Cm-244, Np-237, Pu-238, and U-236 was attributed to INEEL reactor operations. Inventories associated with this waste stream are currently in review. Therefore, the fraction associated with that waste stream was simulated in the LLW pit (Source Area 11) so that the contribution could be readily distinguished from the contribution from RFP waste in the pits (Source Areas 1 through 10).

- Beryllium disposals were assumed to have occurred when reactor core changeouts occurred (i.e., Materials Test Reactor in 1968, Engineering Test Reactor in 1970, and Advanced Test Reactor in 1972, 1977, 1986 and 1987). These disposals are assigned to the soil vault rows (Source Area 13).

Group 1 contaminants were assigned as follows:

- Locations for Am-241 were based on Series-741 sludge data. More than 80% of the Am-241 was contained in the RFP Series-741 sludge. These disposals are divided among the RFP pits (Source Areas 1 through 10) (see Table 5-8 for the distribution of mass among the source areas).

- Neptunium from on-Site disposals was placed in the LLW pit (Source Area 11) beginning in 1958. This allows discriminating the contribution to total risk from on-Site disposal of Np-237 from the contribution of Pu-241 and Am-241 from RFP disposals. Disposals before 1958 went into Trenches 1 through 10 (Source Area 1) (see Table 5-8 for the distribution of mass among the source areas).

- Location for U-233 was based on enriched uranium disposal data. The enriched uranium waste stream was used as a surrogate waste stream identifier because few fuel or scrap shipments were identified. These disposals were primarily assigned to the RFP pits (Source Areas 1 through 10) (see Table 5-8 for the distribution of mass among the source areas).

- Th-229 comes from decay of U-233 and locations were assigned based on the U-233 disposal locations. These disposals were primarily assigned to the RFP pits (Source Areas 1 through 10) (see Table 5-8 for the distribution of mass among the source areas).

Group 2 contaminants were assigned as follows:

- Am-243 mainly came from on-Site disposals. As noted above, Trenches 11 through 58 were not explicitly modeled; therefore, the Am-243 was simulated in the LLW pit beginning in 1958. This approach allowed determining the relative contribution to total risk of the Pu-239 generated by ingrowth separately from Pu-239 disposals from RFP. These disposals are assigned to Source Area 11 (see Table 5-8 for the distribution of mass among the source areas).

- Pu-239 is in several waste streams including sludge, graphite, filters, and noncombustibles. The location of Pu-239 was based on a WasteOScope query for Type V waste, sludge, graphite, and filters. The location of the sludge portion was distributed based on the Series-741 disposals. The graphite portion was distributed based on the graphite disposal information. Locations for filters were similarly assigned. Locations for Type V were used for the remaining noncombustible mass. These disposals are assigned to the RFP pits (Source Areas 1 through 10) (see Table 5-8 for the distribution of mass among the source areas).

Table 5-8. Mass (in grams) disposed of in the 13 simulated source areas by simulation groups for the Subsurface Disposal Area modeling.

Simulation Group	Isotope	Total	Source Area 1	Source Area2	Source Area3	Source Area4	Source Area5	Source Area6	Source Area7	Source Area8	Source Area9	Source Area 10	Source Area 11	Source Area 12	Source Area 13
1	Am-241	5.32E+04	2.07E+03	1.43E+04	1.92E+03	1.18E+04	8.65E+03	2.65E+03	0.00E+00	3.00E+03	6.28E+03	2.56E+03	2.62E-01	0.00E+00	3.45E+01
	Np-237	3.75E+03	1.16E+02	0.00E+00	0.00E+00	0.00E+00	0.00E+00	0.00E+00	0.00E+00	0.00E+00	0.00E+00	0.00E+00	3.63E+03	0.00E+00	0.00E+00
	U-233	1.56E+02	8.51E-06	8.00E-06	0.00E+00	3.19E+01	3.36E-06	2.41E+01	0.00E+00	5.68E-08	6.22E+01	9.98E-01	3.69E+01	0.00E+00	2.12E-02
	Th-229	3.20E-05	4.81E-11	4.52E-11	0.00E+00	1.16E-11	1.90E-11	5.13E-12	0.00E+00	3.21E-13	5.90E-07	2.17E-07	3.07E-05	0.00E+00	4.56E-07
2	Am-243	6.74E+02	3.53E-03	0.00E+00	0.00E+00	0.00E+00	0.00E+00	0.00E+00	0.00E+00	0.00E+00	0.00E+00	0.00E+00	6.74E+02	0.00E+00	0.00E+00
	Pu-239	1.04E+06	9.81E+04	2.36E+05	4.52E+04	1.87E+05	2.76E+05	4.07E+04	0.00E+00	1.42E+04	1.40E+05	7.83E+03	7.78E+01	0.00E+00	0.00E+00
	U-235	2.56E+06	2.15E+05	5.81E+05	0.00E+00	1.98E+05	4.68E+05	3.4,6E+04	0.00E+00	2.41E+03	3.74E+05	4.35E+05	1.38E+05	0.00E+00	1.15E+05
	Pa-231	2.08E-02	5.90E-07	5.55E-07	0.00E+00	1.43E-07	2.33E-07	6.29E-08	0.00E+00	3.93E-09	8.54E-05	3.27E-05	2.07E-02	0.00E+00	3.19E-05
	Ac-227	7.08E-09	0.00E+00	0.00E+00	0.00E+00	0.00E+00	0.00E+00	0.00E+00	0.00E+00	0.00E+00	0.00E+00	0.00E+00	7.08E-09	0.00E+00	0.00E+00
3	Pu-240	7.53E+04	5.99E+03	1.4,7E+04	3.29E+03	1.16E+04	1.75E+04	2.19E+03	0.00E+00	5.86E+02	8.39E+03	7.68E+02	1.03E+04	0.00E+00	0.00E+00
	U-236	4.42E+04	8.35E+03	4.16E+03	4.09E+02	1.39E+03	1.32E+03	5.25E+02	0.00E+00	0.00E+00	1.17E+03	9.91E+02	2.59E+04	0.00E+00	0.00E+00
	Th-232	1.23E+07	1.52E-06	5.35E+06	5.33E+06	4.87E+05	8.82E+05	2.74E+01	9.19E+00	2.76E+01	2.04E+03	1.15E+03	2.36E+05	0.00E+00	7.09E+03
4	Pu-238	9.99E+02	1.05E+01	2.67E+01	6.45E+00	2.95E+01	4.70E+01	2.91E+00	0.00E+00	0.00E+00	1.4,7E+01	1.42E+00	8.59E+02	0.00E+00	0.00E+00
	U-234	0.00E+00	0.00E+00	0.00E+00	0.00E+00	0.00E+00	0.00E+00	0.00E+00	0.00E+00	0.00E+00	0.00E+00	0.00E+00	0.00E+00	0.00E+00	0.00E+00
	Th-230	0.00E+00	0.00E+00	0.00E+00	0.00E+00	0.00E+00	0.00E+00	0.00E+00	0.00E+00	0.00E+00	0.00E+00	0.00E+00	0.00E+00	0.00E+00	0.00E+00
	Ra-226	0.00E+00	0.00E+00	0.00E+00	0.00E+00	0.00E+00	0.00E+00	0.00E+00	0.00E+00	0.00E+00	0.00E+00	0.00E+00	0.00E+00	0.00E+00	0.00E+00
	Pb-210	0.00E+00	0.00E+00	0.00E+00	0.00E+00	0.00E+00	0.00E+00	0.00E+00	0.00E+00	0.00E+00	0.00E+00	0.00E+00	0.00E+00	0.00E+00	0.00E+00
5	U-238	3.4,8E+08	6.31E+07	5.39E+07	1.11E+07	3.23E+07	2.4,8E+07	1.25E+07	0.00E+00	4.84E+05	2.61E+07	1.01E+08	2.32E+07	0.00E+00	0.00E+00
	U-234	1.08E+04	9.69E+02	2.80E+03	1.24E+03	6.80E+02	6.54E+02	2.05E+02	1.82E+02	6.58E+02	1.10E+03	1.21E+03	4.82E+02	0.00E+00	6.25E+02
	Th-230	1.55E+00	3.53E-08	3.68E-08	8.4,8E-09	1.41E-08	1.34E-08	4.24E-09	3.15E-08	1.25E-07	6.10E-07	1.4,8E-01	6.64E-01	0.00E+00	7.38E-01
	Ra-226	6.06E+01	3.68E-13	2.75E+01	2.69E+01	1.33E-02	1.09E-02	2.18E-02	1.28E-02	4.40E-02	8.31E-02	3.78E+00	8.00E-02	0.00E+00	2.13E+00
	Pb-210	6.68E-09	6.4,7E-16	6.72E-16	1.55E-16	2.59E-16	2.4,6E-16	7.76E-17	1.40E-13	5.60E-13	2.82E-12	1.42E-12	6.67E-09	0.00E+00	5.76E-12
6	Nitrate	1.03E+09	2.66E+07	2.84E+07	8.37E+06	4.08E+07	1.23E+07	9.59E+07	0.00E+00	5.55E+06	2.43E+08	5.70E+08	0.00E+00	0.00E+00	0.00E+00
7	Tc-99	3.56E+03	6.01E+02	0.00E+00	0.00E+00	0.00E+00	0.00E+00	0.00E+00	0.00E+00	0.00E+00	0.00E+00	0.00E+00	2.96E+03	0.00E+00	0.00E+00
	1-129	8.94E+02	8.84E+01	0.00E+00	0.00E+00	0.00E+00	0.00E+00	0.00E+00	0.00E+00	0.00E+00	0.00E+00	0.00E+00	8.06E+02	0.00E+00	0.00E+00
	C-14	1.12E+02	9.96E+00	0.00E+00	0.00E+00	0.00E+00	0.00E+00	0.00E+00	0.00E+00	0.00E+00	0.00E+00	0.00E+00	8.57E+01	0.00E+00	1.64E+01
	Cl-36	3.35E+01	9.26E-06	0.00E+00	9.52E+00	0.00E+00	0.00E+00	0.00E+00	0.00E+00	0.00E+00	0.00E+00	0.00E+00	2.40E+01	0.00E+00	0.00E+00
	Nb-94	5.36E+03	2.38E+02	0.00E+00	0.00E+00	0.00E+00	0.00E+00	0.00E+00	0.00E+00	0.00E+00	0.00E+00	0.00E+00	5.12E+03	0.00E+00	0.00E+00

- Location of U-235 was based on disposal data for enriched uranium. These disposals are primarily assigned to the RFP pits (Source Areas 1 through 10) (see Table 5-8 for the distribution of mass among the source areas).

- Location of Pa-231 was based on disposal data for enriched uranium. These disposals are primarily assigned to the RFP pits (Source Areas 1 through 10) (see Table 5-8 for the distribution of mass among the source areas).

- Location of Ac-227 disposals was assumed to be in the LLW pit. These disposals are assigned to Source Area 11 (see Table 5-8 for the distribution of mass among the source areas).

Group 3 contaminants were assigned as follows:

- The portion of the Pu-240 generated by INEEL reactor operations was disposed of in the LLW pit (Source Area 11) for disposals after 1958. The RFP portion of Pu-240 was proportioned with a methodology similar to the Pu-239 in Group 2 above. The fraction of the waste in the various RFP waste streams was used to determine distribution of masses into the various RFP pits (Source Areas 1 through 10) (see Table 5-8 for the distribution of mass among the source areas).

- Because U-236 has on-Site contributions, locations were determined using the same approach applied for plutonium. All waste was assumed to have been placed in trenches (Source Area 1) through 1958. The U-236 was divided between the RFP waste in pits (Source Areas 2 through 10) and on-Site waste in the LLW pit (Source Area 11) (see Table 5-8 for the distribution of mass among the source areas).

- Th-232 is assumed to come primarily from decay of U-236 so disposals are proportioned in source areas based on the U-236 distribution.

Group 4 contaminants were assigned as follows:

- Waste was proportioned similar to plutonium waste in Groups 2 and 3 because significant contributions of Pu-238 may have been received from the INEEL reactor operations. The on-Site portion of the Pu-238 was disposed of in the LLW pit (Source Area 11) for disposals after 1958. The RFP portion of Pu-238 proportioned with a methodology similar to the Pu-239 in Group 2 above (see Table 5-8 for the distribution of mass among the source areas).

- Disposal inventories of U-234 and its daughters (i.e., Th-230, Ra-226, and Pb-210) are included in Group 5; therefore, inventory was zero for Group 3 to allow discriminating the relative contribution to total risk from the uranium disposals and the U-234 ingrowth from Pu-238.

Group 5 contaminants were assigned as follows:

- The bulk of U-238 and U-234 was in roaster oxide. Disposal data for roaster oxide exist for 1966 through 1969. Before 1961, all waste was disposed of in the open pit or trench. From 1962 to 1965, mass was proportioned equally in the open pits. All uranium waste from 1970 to 1978 was disposed of on Pad A. Uranium waste disposal after 1978 was assigned to the LLW pit. Because the majority of the uranium disposals are from RFP, these disposals were assigned to Source Areas 1 through 11 (see Table 5-8 for the distribution of mass among the source areas).

- Inventories of Th-230, Ra-226 and Pb-210 are assumed to come largely from ingrowth from the uranium decay chain and are proportioned in the pits and trenches in the same manner as U-238.

Group 6 contaminants were assigned as follows:

- Nitrates were primarily in the Series-745 sludge. The Series-745 data were used for disposals from 1967 through 1978. Disposal before 1967 were proportioned into Pits 1 through 10. Waste disposal beginning in 1979 was assigned to the LLW pit. These disposals were proportioned between Source Areas 1 through 11 (see Table 5-8 for the distribution of mass among the source areas).

Group 7 contaminants were assigned as follows:

- The amount of Tc-99 in beryllium blocks is small. It was modeled as surface washoff rather than dissolution because part of the Tc-99 is in activated metal and DUST-MS cannot handle two separate corrosion rates in a single year. Therefore, the Tc-99 was assigned to Trenches 1 through 10 for disposals before 1960 (Source Area 1) and in the LLW pit for disposals after 1960 (Source Area 11) (see Table 5-8 for distribution of mass among the source areas).

- I-129 comes from on-Site generators. Disposals of I-129 before 1960 were in Trenches 1 through 10 (Source Area 1) and disposals after 1960 were placed in the LLW pit (Source Area 11). Distribution of mass among the source areas is shown in Table 5-8.

- C-14 consists of several waste types: beryllium blocks, activated metal, and other trash. Before 1960, the C-14 was disposed of in Trenches 1 through 10 (i.e., Source Area 1). Disposals after 1960 were segregated to evaluate the effect of the C-14 in the beryllium blocks and to be able to account for the different corrosion rate of beryllium compared to stainless steel. The C-14 disposed in the beryllium blocks was disposed of in the **SVRs** (i.e., Source Area 13) and the C-14 in activated metal and other trash was put into the LLW pit (i.e., Source Area 11) because Trenches 11 through 58 were not explicitly modeled.

- Most of the C1-36 is contained in the beryllium blocks that were disposed of in the **SVRs** (Source Area 13). Disposals for off-Site waste were in Pit 3 (Source Area 3) and in trenches before 1961 (Source Area 1). The remainder was assigned to the LLW pit (Source Area 11) because the later trenches, Trenches 11 through 58, were not modeled explicitly (see Table 5-8 for distribution of mass among the source areas).

- Nb-94 came from on-Site generators. Because none of the Nb-94 is in the beryllium blocks, Nb-94 disposals were modeled as in the trenches (Source Area 1) or LLW pit (Source Area 11). The LLW pit was used rather than the soil vault rows to allow consistency with other contaminants in the group that simulated the contribution from the beryllium blocks in the **SVRs** (see Table 5-8 for the distribution of mass among the source areas).

Based on these assumptions, the mass disposed of in each of the 13 source areas is listed by simulation group in Table 5-8.

5.1.6 Infiltration Rates

Site-specific infiltration rates were developed for the SDA. The infiltration rate assigned to each of the 13 source areas was based on the assignment of infiltration in the subsurface flow and transport model. Infiltration rates applied to the grid blocks of the subsurface flow and transport model along with the 13 source areas are presented in Figure 5-2. Infiltration assigned in the subsurface model was averaged over the grid blocks representing the source areas. The resulting averages are shown at the bottom of Figure 5-2.

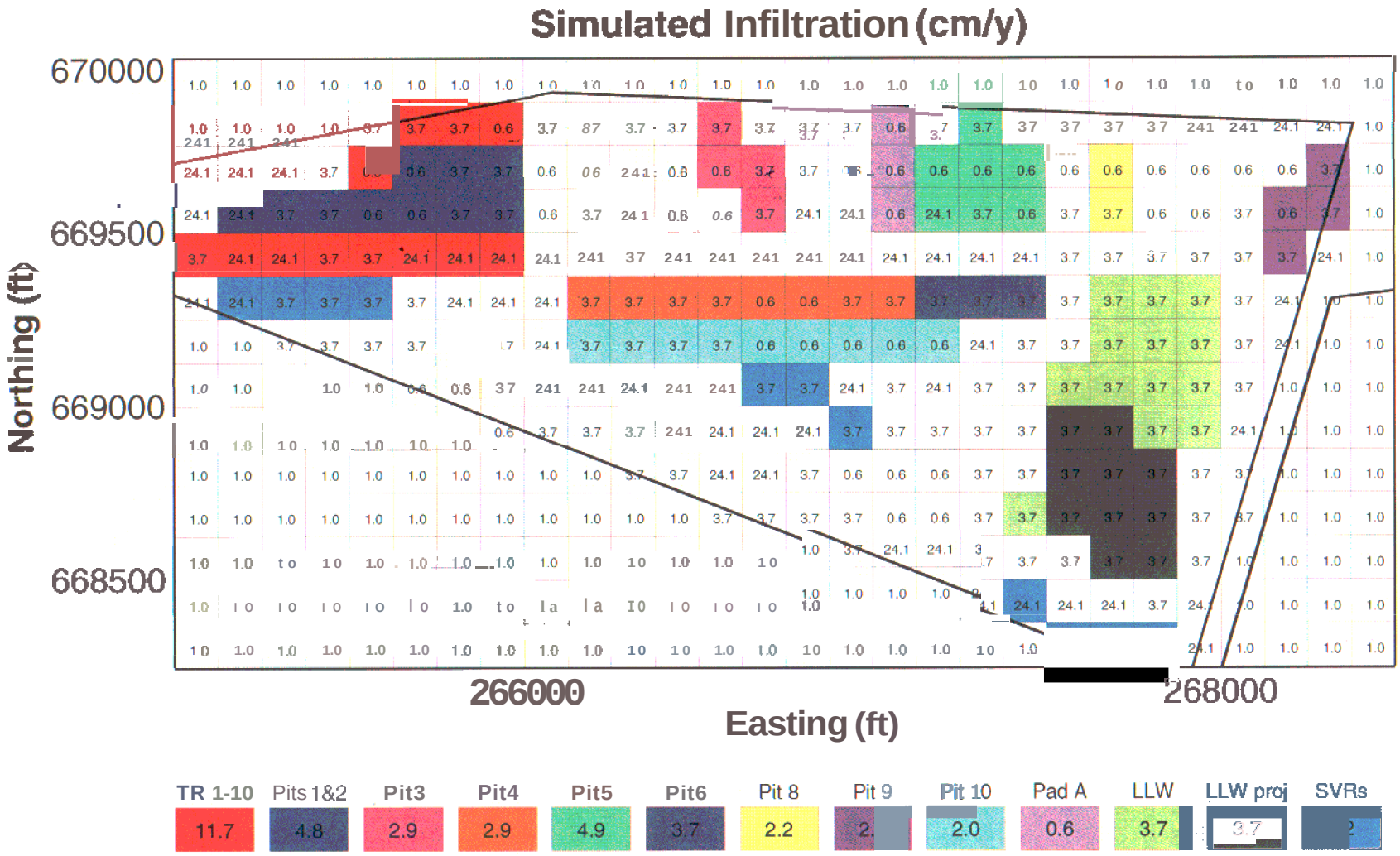

Figure 5-2. Infiltration rates assigned in the subsurface flow model and averages used for the 13 source areas simulated in the source release model.

5.1.7 Source Term Model Calibration

Monitoring data from in and immediately proximal to the buried waste are required to calibrate the source term model. Data taken from directly beneath the waste are limited and time histories have not been developed. Therefore, available data are insufficient to attempt source term model calibration.

Several different types of probes were installed in the waste as described in Section 3.6. Continued monitoring and evaluation of the data could allow validation of the values used in the ABRA source release modeling and provide data sets for calibrating any future source release modeling.

5.2 Dissolved-Phase Transport Modeling

Contaminant fate and transport simulations performed for dissolved or aqueous phase COPCs are discussed in this section. Volatile organic compound modeling is addressed in Section 5.3. The model developed and implemented to represent movement of water and contaminants in the subsurface for this ABRA was derived from the model presented in Magnuson and Sondrup (1998), which was used to support development of the IRA (Becker et al. 1998). The model originally developed by Magnuson and Sondrup (1998) for the IRA will be referred to as the IRA model. The IRA model was improved to represent the current best interpretation of water movement and contaminant transport in the subsurface. The ABRA numerical model described in this section was developed and implemented to represent movement of water and contaminants after they are released from their disposal locations. This section presents the conceptual model, improvements compared to the IRA model, the basis for parameters of the numerical model, and results of the numerical model in terms of moisture distributions and resulting contaminant concentrations.

5.2.1 Dissolved-Phase Flow and Transport Conceptual Model

The general conceptual flow model treated water movement as though subsurface sediments consisted of a heterogeneous, isotropic, porous medium. Net infiltration of meteoric water into the subsurface was described in the model by three constant rates representing areas of low, medium, and high infiltration. Surficial sediments and sedimentary interbeds were simulated with varying thicknesses and upper-surface elevations. Only the three uppermost interbeds were considered in the conceptual model. These were the A-B, B-C, and C-D interbeds. Interbeds deeper than the C-D interbed, though present in reality, were not included in the ABRA simulations.

Flow in the fractured basalt portion of the subsurface was considered as occurring only in the fracture network, to emulate an anisotropic medium with a low effective porosity and a high permeability. The basalt matrix itself was not considered to affect flow or transport.

The effect of water migrating laterally at depth in the vadose zone from either Spreading Area A or B, or from the Big Lost River was included in the conceptual model. No attempt was made to discern the source. Rather, based on the 1999 USGS tracer test (Nimmo et al. 2002), the influence of this additional spreading-area water was limited to the western half of the SDA. A steady-state spreading area influence was modeled; however, in reality, the effect would vary temporally, depending on the magnitude of surface water flows in the Big Lost River and discharges to the spreading areas. Variation caused by changing the steady-state magnitude of the spreading area influence in the vadose zone model was assessed in sensitivity cases.

Movement of water and contaminants within the aquifer was considered controlled by the regional flow in the aquifer. Because of the long time durations of hundreds to thousands of years simulated in the ABRA, movement of water within the SRPA was considered steady state.

Locally, groundwater flow was affected by a region of low permeability in the aquifer. This region has been identified in wells immediately south of the SDA. This low-permeability region may extend underneath the SDA, as evidenced by the extremely slow decline in concentration of a tracer injected directly into aquifer Well M17S. This extremely slow decline is indicative of low velocities at that location. Low velocities in the aquifer have an impact on model results. As contaminants enter the aquifer from the vadose zone, less dilution occurs in grid blocks with low aquifer velocities and simulated contaminant concentrations are higher than they would be if the aquifer velocity were greater.

Processes that were considered for dissolved-phase transport include advection, dispersion, diffusion, radioactive chain decay and ingrowth, and adsorption in the sediment portions of the simulation domain.

In the fractured basalt portion of the simulation, no sorption was assumed. Sorption in surfkial and interbed sediments was assumed to follow linear reversible isotherms that could be described by use of partition coefficients (K_ds). Sediment K_ds were assigned based on best-estimate values rather than conservative screening values. A set of best-estimate K_ds developed by Dicke (1997) was the primary source used in this application. Revised values for C-14 were included based on additional RWMC-specific work conducted since 1997 (Dicke 1998). Facilitated transport mechanisms (e.g., colloidal transport) may affect contaminant migration in the SDA subsurface. Studies have been conducted that show very small fractions of the plutonium and americium may move in a facilitated manner at the SDA (Grossman et al. 2001) (see Section 3.7). Facilitated transport was included conceptually in sensitivity studies. In the baseline case, facilitated transport was not included in the conceptual model and its implementation.

Single isolated detections of contaminants have occurred at the SDA during monitoring of subsurface contaminants. Though these isolated detections may be indicative of contaminant transport, it is not feasible with the current modeling approach to try to emulate each one. Instead, the subsurface transport model attempts to mimic the large-scale overall behavior of contaminants in the subsurface. This approach directs the model to emulate Contaminants that are consistently present in a distributed manner in the subsurface.

Concentrations of contaminants in the aquifer near the SDA are not attributed to facilities in the general upgradient direction relative to flow in the aquifer. This interpretation is based on analyses of time histories of contaminant-monitoring results in the upgradient well-monitoring network. The implication of this aspect of the conceptual model is that if contaminants are in the aquifer near the SDA, then the contamination originated in the SDA and was derived from leaching and migration of contaminants from the buried waste.

5.2.2 Predecessor Model, the Interim Risk Assessment

Though other attempts have been made to simulate flow and transport of specific contaminants in the subsurface of the SDA, the primary previous modeling study was the comprehensive model developed by Magnuson and Sondrup (1998) for the IRA. That model represented the first attempt to simulate flow and transport through the entire vadose zone and aquifer domains for an extensive suite of contaminants of potential concern. The IRA model attempted to include calibration to vadose zone perched water behavior and an interpreted contribution to nitrate concentrations in the aquifer. Results of that calibration were termed limited in their degree of success in emulating observed behavior. Attempts to improve calibration were hindered by the paucity of vadose zone monitoring data that could be used to demonstrate transport of a nonsorbing contaminant. The IRA model was used to make a series of 10,000-year predictive simulations for 52 contaminants. Results of that modeling formed the basis for risk estimates in the IRA and were used to screen contaminants for the **ABRA.**

The IRA model was slightly revised for the ABRA by Sondrup (1998) to improve simulation of VOCs (see Section 5.4). The IRA model also has been used by Waste Management to update both the LLW Radiological Performance Assessment (Case et al. 2000) and the Composite Analysis (McCarthy et al. 2000). The IRA model development, implementation, and results have undergone extensive review by Fabryka-Martin, Gee, and Flint (1999) and the USGS (1998). Though the reviews are generally complimentary of the IRA model, none of these reviews concluded that the IRA model was in a satisfactory state to make conclusive predictions of the fate and transport of contaminants in the subsurface. Of these reviews, the USGS effort (which is currently in progress) was by far the most extensive. The main comments from the USGS about modeling flow and transport of radionuclides at the RWMC are listed below:

- The modeling performed for the IRA cannot necessarily be shown to be conservative.
- Spatial variability of hydrologic and transport properties of the sedimentary interbeds should be evaluated and the impact of including this spatial variability into the modeling should be assessed.
- Impacts of additional sources of vadose zone water from the Big Lost River system on predicted contaminant concentrations should be evaluated.
- Selected K_d values used in the IRA cannot be shown to be conservative because they do not account for (a) colloidal transport, (b) the enhanced mobility fraction observed in column studies, (c) variations in mineralogy, (d) nonlinearity of isotherms, and (e) fluctuations in pore water chemistry. Furthermore, K_d values taken from the literature cannot be shown to be representative of the SDA.

Modeling presented in Section 5 responds to each of these observations, particularly to the second and third bullets above.

5.2.3 Overview of Improvements to the Interim Risk Assessment Model

Improvements on the IRA model that have been made in large part in response to review comments are summarized below.

5.2.3.1 Vadose Zone and Aquifer Domain Separation. The IRA model had both the vadose zone and the aquifer included into a single simulation domain to enable simulating off-gassing of volatile contaminants as they migrated within the aquifer. While this approach was convenient because it eliminated the need for an interface to take water and contaminants from the bottom of the vadose zone model and assign them as boundary conditions at the top of a saturated zone model, the single domain was computationally inefficient because of the larger scale required to include the INEEL southern boundary in the simulation domain. This inefficiency resulted in an excessively large number of grid blocks in portions of the vadose zone distant from the SDA that were not of interest.

By separating the vadose zone and aquifer into two domains, increased discretization could be achieved in the representation for the vadose zone with emphasis on the surfkial sediments. The smallest horizontal grid used to represent surface sediments were square grid blocks that were 38.1 m (125 ft) on a side. By comparison, the smallest grid blocks in the IRA model were 62.5 m (205 ft) on a side. This increased discretization allowed improved representation of the release of different waste streams into the subsurface.

5.2.3.2 Conformable Gridding in the Vadose Zone Model. The IRA model had a rigidly structured three-dimensional grid where the vertical dimension of each grid in a horizontal slice of the

model was the same. This structure precluded accurately representing the elevation of the lithologic contacts between interbed sediments and basalts in the simulation domain. In the ABRA model, the grid blocks had variable vertical dimensions to better emulate the actual lithologic surfaces. This conformable grid also had a variable upper surface elevation. The IRA model treated the upper surface as perfectly flat.

5.2.3.3 *Improved Linkage Between Source Release and Vadose Zone Models.* The current model is similar to the IRA model and relies on an external simulation of the release of contaminants from their burial locations. The IRA source model applied one overall average infiltration rate of 8.5 cm/year (3.3 in./year) to calculate the release of contaminants. However, the IRA subsurface model included spatially varying infiltration across the surface of the SDA. In the current model, the spatially varying infiltration rates were partially incorporated into the source term model. The assigned infiltration rates for the grid blocks representing a waste stream were averaged together to determine a more consistent estimate of the amount of water going through that portion of the model. This resulted in 13 infiltration rates being used in the source term model instead of one (see Figure 5-2). The effect of this improvement was tested in a sensitivity analysis.

5.2.3.4 *Additions to Lithologic Database and Spatial Variability Assessment.* Twenty-two wells at 13 locations have been drilled and completed since the IRA model was developed. Most of these wells were drilled in response to the USGS review of the IRA modeling. Lithologic information from these additional wells was used to further interpret local lithology. The IRA model included a spatial variability assessment that was used to krige lithologic contacts and assign material properties in the simulation grid. The spatial variability assessment was upgraded for the current model and the final kriged results were validated in Leecaster (2002).

5.2.3.5 *Aquifer Model Calibration.* Water levels and flow directions for the aquifer simulations were recalibrated with the additional data collected after the development of the IRA model. Complete details of aquifer model development and calibration are contained in Whitmire (2001).

Recalibration of the aquifer model was necessary to take advantage of seven additional water-level data from aquifer monitoring wells that were not present for the calibration of the IRA model. The additional aquifer wells were designated M11S, M12S, M13S, M14S, M15S, M16S, and M17S. Deviation (i.e., corrected water) level data were used from two time periods in calendar year 2000. An optimal set of aquifer permeabilities were selected that minimized differences between measured and simulated water levels. This optimized set of parameters was used in predictive modeling for the ABRA. As part of this aquifer calibration effort, kriged permeability distributions based on single well pump-test results were tested. However, the short spatial correlation range and limited data points did not result in an accurate prediction of water levels.

The effect of transient influences from the spreading areas also was investigated. Simulation results indicated that, when additional water representing recharge from the spreading areas was input into the aquifer, the magnitude of southeasterly groundwater-flow velocities beneath the eastern portion of the SDA increased; however, the directions changed only slightly.

The flatness of the water table coupled with an apparent low-permeability region to the south-southwest of the SDA precludes accurate determination of groundwater-flow directions. The IRA hypothesis that the flow velocities immediately under the SDA are slow is consistent with new evidence. The ongoing tracer test in Well M17S immediately beneath the SDA has been showing a very slow dilution of tracers introduced directly into the well, which is indicative of slow movement.

This hypothesis also is consistent with the interpretation by Roback et al. (2001) that the RWMC is in a low-permeability region that extends southerly from the Lost River Range onto the INEEL.

Additional water levels collected during the ongoing WAG 7 quarterly monitoring program will be a key part of conclusively determining direction and timing of aquifer flow velocities in the SDA region.

5.2.3.6 Contaminant Data. The IRA model was primarily based on monitoring data collected before April 1995. Additional contaminant monitoring data were available from previously existing wells and new vadose zone and aquifer wells for use in developing the current model. As discussed in Section 4, the data from the monitoring network do not indicate consistent trends in the vadose zone or aquifer. The generally sporadic monitoring results could not be used as a basis for calibrating a numerical simulation.

5.2.3.7 Hydrologic and Transport Data. Interbed core samples from the 22 wells that were drilled in 1999 were collected for analysis of hydrologic and transport properties. These analyses generated an order of magnitude improvement in the size of the data set available for spatial variability analyses, especially for hydrologic properties. Correlation ranges for the data were determined and used to predict spatially variable properties for the B-C and C-D interbeds. Including these spatially variably hydrologic properties was necessary to address the USGS criticism of the IRA that disregarding spatial variability in interbed properties neglected the possibility of fast migration pathways through the interbeds.

Tensiometers were installed at each location where a suction lysimeter was installed in the B-C and C-D interbeds. Matric potential data from the tensiometer network can be used to (a) guide timing of sampling activities, (b) determine the vertical extent of transient infiltration events at the surface, and (c) determine timing and extent of the influence of discharges to spreading areas in the vadose zone beneath the SDA.

Transport property analyses on approximately 60 interbed cores included sorption isotherms for uranium and neptunium; particle size distributions; surface area; exchangeable cations and anions; clay mineralogy; and extractable silica, iron, manganese, and aluminum. Comparison of partition coefficients from the sorption isotherms to the values from Dicke (1997) support the conclusion that the partition coefficients selected for simulating transport of uranium and neptunium are physically plausible and conservative because they are on the extreme lower end of the measured partition coefficient distributions. Sorption isotherms measured from the core samples were decidedly nonlinear. Partition coefficients with linear isotherms were used in the simulations. Comparisons of the linear values to the nonlinear values also demonstrated that linear values were conservative with respect to enhancing transport over the range of simulated concentrations.

5.2.4 Baseline Model Development and Description

Development and parameterization of models used to simulate flow and transport in the subsurface are described in this section, which also includes a complete list of assumptions. The vadose zone model is described first, followed by the aquifer model.

5.2.4.1 Assumptions. This section lists all assumptions that resulted from the conceptual model (discussed above) or were necessary to develop the subsurface model. Assumptions are divided into flow and transport categories. Most of these assumptions were the same as those used in developing the IRA model. ***Assumptions that were modified are italicized.*** These assumptions were applied only to dissolved-phase subsurface flow and transport modeling. Assumptions relative to source term modeling and VOC modeling are included in Sections 5.1 and 5.4, respectively.

5.2.4.1.1 Flow Modeling Assumptions

- Infiltration was spatially variable inside the SDA and was greater than the infiltration that occurs outside the SDA because of disturbed soil profiles with reduced vegetation.

- The infiltration description of Martian **(1995)** was adequate for the ABRA model and, beginning in **1952,** was implemented as though it was effective across the SDA.

- The background infiltration rate outside the SDA through undisturbed vegetated sediments was 1 cm/year **(0.4** in./year).

- Initial conditions obtained from simulating a background infiltration rate of 1 cd year **(0.4** in./year) for **100,000** days (approximately **274** years) were adequate for representing the vadose zone beneath the SDA.

- The amount of water entering the SDA from the three historical floods was adequately estimated by Vigil **(1988).**

- Duration of infiltration from each of the historical flooding events was **10** days.

- Infiltration patterns at the SDA will remain the same indefinitely into the future.

- The high infiltration rate assigned over parts of the SDA by Martian **(1995)** was sufficient to account for occasional flooding of the SDA that may occur in the future.

- The surficial sediments and sedimentary interbeds have spatially variable lithologic surfaces and thicknesses that influence water and contaminant movement.

- Interbeds below the C-D interbed are thin and discontinuous and do not significantly affect flow and transport near the SDA.

- Hydrologic properties in the surficial sediments and A-B interbed were homogeneous. ***Hydrologic properties in the B-C and C-D interbeds were heterogeneous and varied spatially.***

- Waste had the same hydrologic properties as the surficial sediments.

- Flow in the fractured porous basalts was controlled by the fracture network and could be adequately represented as a high-permeability, low-porosity equivalent-porous continuum using a Darcian description.

  The field-scale hydraulic properties for fractured basalts were adequately described by the inverse modeling performed by Magnuson **(1995)** for the large-scale infiltration test.

  A steady-state influence in the vadose zone model occurred because of Big Lost River water discharges to the spreading areas. The ABRA model implements additional water entering the simulation domain just above the C-D interbed and includes enough water to affect the western portion of the C-D interbed beneath the SDA.

- ***Spreading area influence on the vadose zone began in 1965, as that was the year when the first significant flows in the Big Lost River occurred after the diversion dam was constructed in 1958 (Wood 1989).***

- Water movement in the aquifer was steady-state. Possible influences of discharges from the Big Lost River to the spreading areas do not influence flow in the aquifer in the immediate vicinity of the SDA.

- ***Water levels corrected for borehole deviations from FY 2001 were adequate for calibrating the SRPA model and are representative of long-term steady-state conditions.***

- A region of low permeability exists in the aquifer southwest of the SDA.

- The effective depth of the SRPA is 76 m **(250** ft) (Robertson **1974)**

5.2.4.1.2 Transport Modeling Assumptions

- Field-measured concentrations of COPCs are generally representative and valid based on data quality requirements associated with sampling activities. Single isolated detections of contaminants are anomalous and not representative because they are not consistently present.

- Advection, dispersion, diffusion, sorption, and radioactive decay are the only processes that influence dissolved-phase contaminant movement in the subsurface beneath the SDA.

- A linear equilibrium reversible partition coefficient is representative of all geochemical processes that occur between contaminants dissolved in water and sediments.

- Partition coefficients are homogenous in the interbeds.

- ***Sorption does not occur in fractured basalt portions of the vadose zone and aquifer.***

- There were no upgradient influences from other INEEL facilities on aquifer contaminant concentrations near the SDA, with the exception of nitrate, which had an estimated local background concentration of **0.7** mg/L.

5.2.4.2 Simulation Code. The TETRAD code (Vinsome and Shook **1993),** Version **12.7,** was used to simulate flow and transport for the ABRA. The TETRAD code has complete multiphase, multicomponent simulation capabilities and can mimic the behavior of any number of components in aqueous, gaseous, and oleic phases. The ABRA modeling was limited to dissolved phase aqueous transport using the TETRAD block-centered finite-difference approach and local grid refinement. Though modeling was not performed in the ABRA for VOCs, the IRA VOC modeling results were adapted for use in the ABRA as discussed in Section **5.3.**

Dual-permeability simulation capabilities used to simulate transport in both aqueous and gaseous phases in the IRA model were not applied in this modeling exercise. Instead, as discussed in Section **5.3,** the results of the vapor phase modeling for the IRA were linearly scaled.

A limitation of using TETRAD is that it treats dissolved-phase contaminants as a separate water component and tracks their movement as if the contaminants were a portion of the total water mass. When contaminants are added into a model representation, they can potentially increase total water in the system. For cases in which contaminant concentration is very low, such as for dissolved radionuclides, the contaminant mass must be scaled upwards from one to **10** orders of magnitude to result in a mole fraction large enough to provide satisfactory mass balance tracking while still maintaining a small enough mole fraction as to not affect the water pressure field. This method effectively limits the valid range of a transport solution to a region around the center of mass of a propagating contaminant front and a limited

portion of the leading and trailing tails of the distribution that are above the specified convergence criterion. Additional complications are introduced when a contaminant sorbs because removal of its related water mass can affect the simulated pressure field. When a decay chain is simulated, all the members of the decay chain must be equivalently scaled.

5.2.43 Vadose Zone Flow Model

5.2.4.3.1 Horizontal Domain Extent and Discretization—Two domains were considered for simulating vadose zone flow and transport (see Figure 5-3). An initial attempt was made to use a vadose zone domain that included the spreading areas, which would have allowed spreading area fluxes to be input at their actual locations at the surface. This initial attempt was unsuccessful because the number of grid blocks became too great and increased the computational burden to the point where the simulation was not feasible.

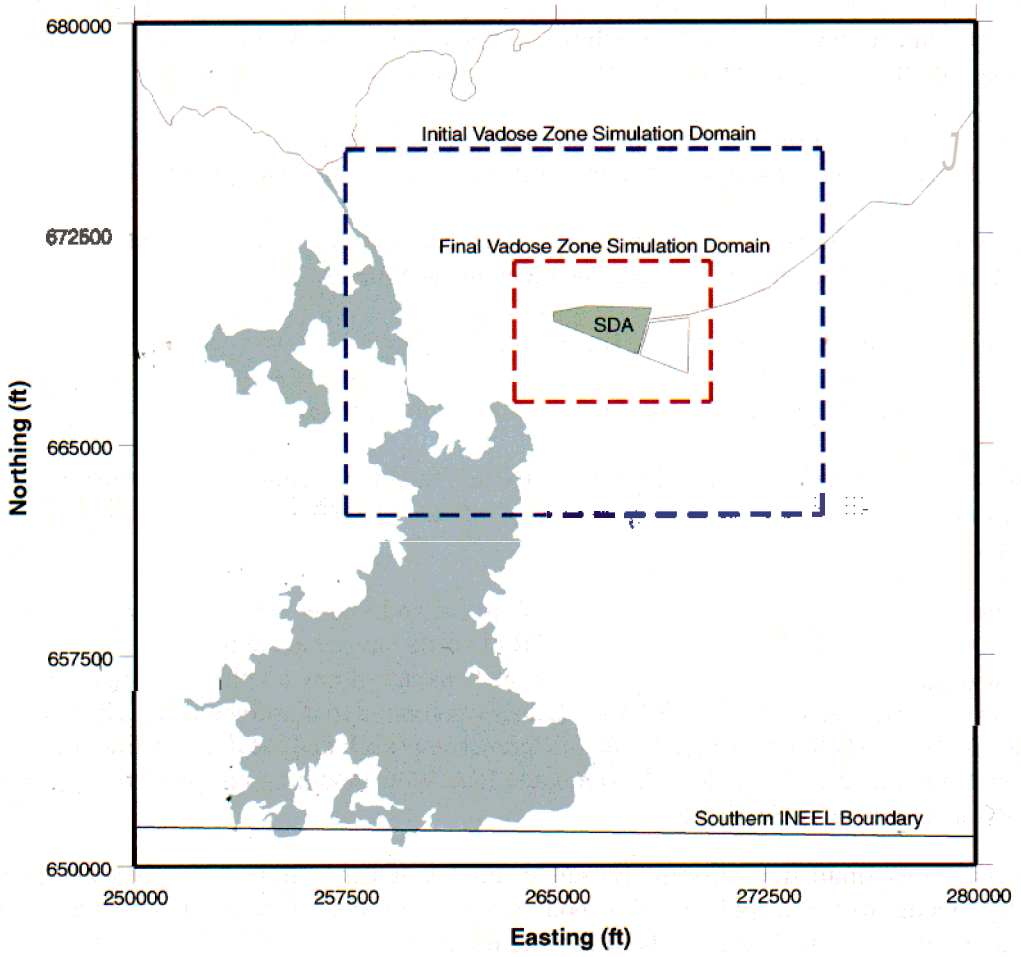

Figure 5-3. Horizontal domains considered for simulation of vadose zone flow and transport.

Horizontal gridding for the final vadose zone domain is shown in Figure 5-4. The upper part of the figure shows just the domain. Two concentric levels of refinement are used to obtain adequate grid resolution in the SDA. The largest horizontal grids are 152.4 m (500 ft) on a side and the smallest grid blocks are 38.1 m (125 ft) on a side. The lower part of the figure shows the same domain with well locations superimposed on the grid. Selection of the grid domain required a balance between the objectives of maximizing the extent of the domain so that outlying wells such as Wells M7S, M15S, and M16S could be included while still obtaining sufficient resolution in the SDA. As shown in Figure 5-4,

some outlying wells were not encompassed in the vadose zone simulation domain. The final domain extent was adequate to simulate transport without undue influence from the horizontal no-flux boundaries, causing elevated simulated concentrations at the boundaries.

5.2.4.3.2 Lithologic Assignment — With the addition of the 22 wells drilled in 1999, 118 wells currently exist in the SDA region from which lithologic information could be used for interpreting lithology. These wells are shown in Table 5-9. The table shows the upper surface and thickness for the surficial sediments and the A-B, B-C, and C-D interbeds. Interbeds deeper than the C-D interbed were not simulated. The lithologic data were derived from the USGS database developed by Anderson et al. (1996) with additions for wells drilled in 1999. *An* entry of a "-" symbol in Table 5-9 indicates that either the interbed was absent or lithologic information could not be extracted from the data. The latter is the case, for example, in Well I-1D where no attempt was made to obtain the depth of the A-B and B-C interbeds because the well was drilled to obtain lithologic information for the C-D interbed. An entry with a ">" symbol following it indicates partial penetration of an interbed. Three wells (i.e., Wells 6E, 7E, and DE1) were drilled but did not have information available for the lithologic spatial analysis and are not included in the table.

An extensive spatial variability assessment was performed on this data set (Leecaster 2002) using Splus Version 1.5 (MathSoft 2000). The first stage of this stepwise analysis consisted of calculations and modeling to determine the best empirical variograms for raw data and residuals followed by directional variogram analysis to investigate statistical anisotropy, variogram clouds, and models of resulting isotropic data. The next stage was to predict the upper elevations and thicknesses of the surficial sediments, and the A-B, B-C, and C-D interbeds for each of the base and refined grids in the model domain. The three spatial models used to predict values for the base and refined grids were inverse distance weighting, simple kriging, and universal kriging. Cross validation was performed to assess the fit of the models for the variogram modeling and the kriging predictions. Results were selected based on the model that was most accurate and plausible. The statistical testing performed in this analysis included testing different methods for handling cases of partial penetration and gaps.

Table 5-10 gives the final fitted variograms and interpolation method used for each of the lithologic variables. The final fitted variograms for all the lithologic variables used a spherical form. These fitted variograms were used to krige the upper surfaces and thicknesses for the surficial sediments and the A-B, B-C, and C-D interbeds onto the base grid and each of the refined grids.

Figures 5-5, 5-6, 5-7, and 5-8 show examples of kriged surfaces for lithologic contacts and thicknesses. The well locations and lithologic elevation or thickness also are shown. The kriged surfaces were used in developing the vertical conformable grids discussed in the next subsection. One advantage of kriging is the ability to estimate uncertainty in the results. The uncertainty in the elevation of the surficial sediments is included in Figure 5-5. A complete set of kriging standard error plots are included in Leecaster (2002), and generally shows greater uncertainty at distance from the measurement locations. Estimates were kriged for grid block centroids, which means that for a grid block containing a well showing an interbed gap, the kriged result may not show that same gap. Where gaps were statistically significant, they persisted through the kriging as evidenced in the thickness of the A-B interbed (see Figure 5-6). Where gaps were less consistent, such as in the B-C interbed thickness plot, the gaps influenced the kriged surfaces but no gaps persisted into the kriged results (see Figure 5-7).

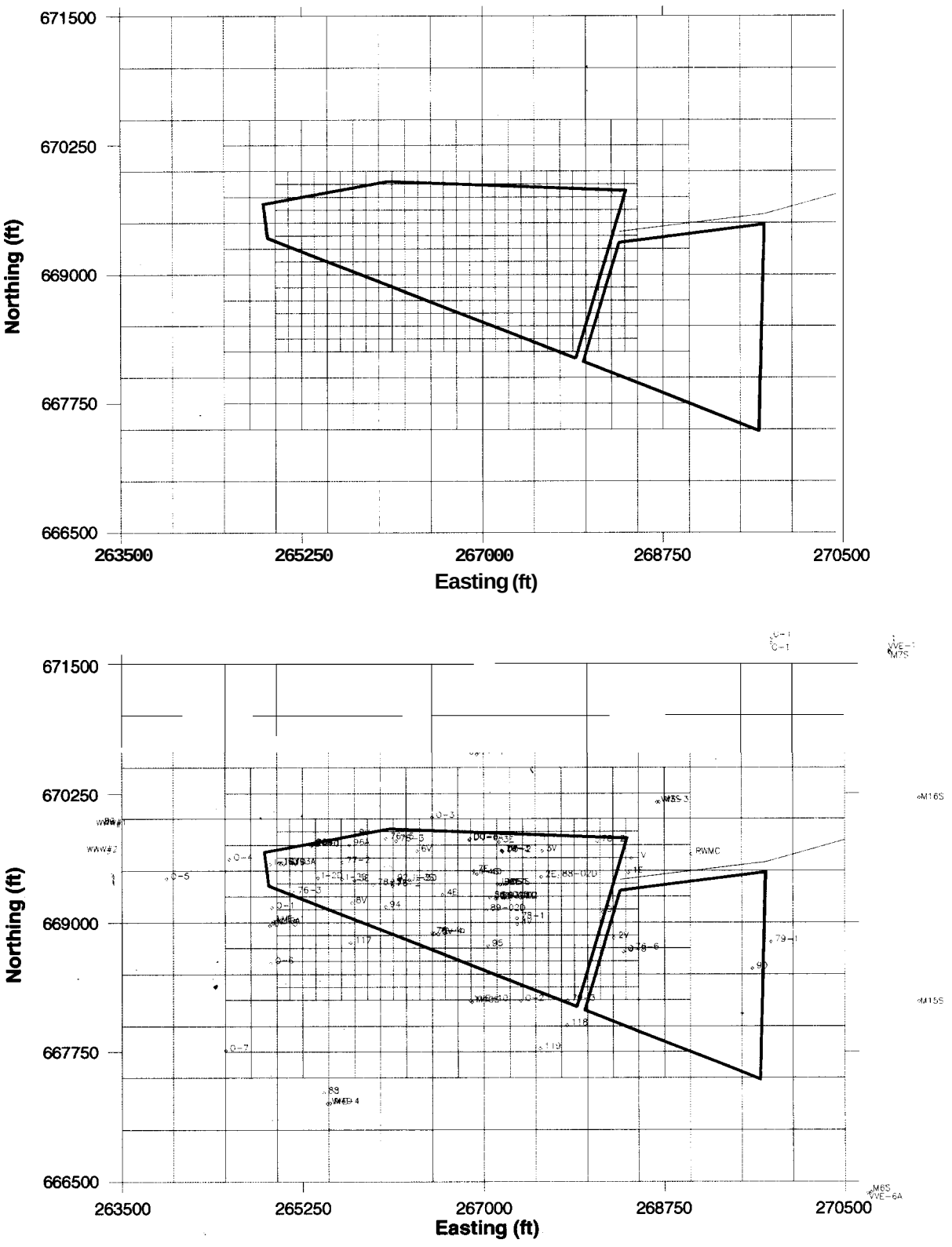

Figure 5-4. Horizontal discretization for the vadose zone model domain.

Table 5-9. Lithologic data used for FY 2001 vadose zone model for the Subsurface Disposal Area baseline risk assessment.

Common Well Name	Northing (ft)	Easting (ft)	Surface Elevation (ft amsl)	Thickness (ft)	A-B Interbed Elevation (ft amsl)	Thickness (ft)	B-C Interbed Elevation (ft amsl)	Thickness (ft)	C-D Interbed Elevation (ft amsl)	Thickness (ft)
76-1	669749	265343	5,009	7	4,983	9	4,921	0	4,790	9>
76-2	669352	266118	5,010	12	4,989	4	4,924	0	4,789	32>
76-3	669286	265161	5,010	18	4,988	3	4,917	26	4,790	20>
76-4	668889	266520	5,011	7	4,995	7	4,915	4	—	—
76-4a	668896	266495	5,011	2	4,995	8	4,915	3	4,790	33>
76-5	669808	266055	5,011	11	5,000	0	4,918	17	4,791	20
76-6	668734	268426	5,011	4	5,007	0	4,913	4	4,783	6
77-1	670623	266933	5,017	4	4,977	8	4,919	6	4,789	22
77-2	669579	265633	5,014	18	4,986	3	—	—	—	—
78-1	669037	267319	5,010	15	4,995	0	—	—	—	—
78-2	669782	268099	5,007	2	4,989	5	4,914	7	4,784	30>
78-3	669788	266151	5,011	4	4,999	0	4,919	0	4,786	23>
78-4	670650	266935	5,018	2	4,976	5	4,920	7	4,790	20
78-5	669365	265931	5,010	12	4,998	0	4,915	28	4,790	30>
79-1	668807	269783	5,010	5	5,005	0	4,897	28	4,785	5
79-2	669692	267171	5,011	13	4,987	3	4,913	4	—	—
79-3	668243	267807	5,008	13	4,995	0	4,909	4	4,780	29
88-02D	669441	267717	5,006	6	4,981	3	4,912	8	—	—
88-01D	669240	267059	5,008	18	4,990	0	4,907	4	4,781	5>
89-01D	669233	267132	5,009	22	4,987	0	4,908	7	4,781	14>
89-02D	669114	267021	5,011	16	4,995	0	4,910	9	4,780	7

Table 5-9. (continued).

Common Well Name	Northing (ft)	Easting (ft)	Surface Elevation (ft amsl)	Thickness (ft)	A-B Interbed Elevation (ft amsl)	Thickness (ft)	B-C Interbed Elevation (ft amsl)	Thickness (ft)	C-D Interbed Elevation (ft amsl)	Thickness (ft)
93-01	669228	267112	5,009	20	4,989	0	4,903	4	4,781	10>
93-02	669234	267197	5,009	29	4,980	0	4,902	6	4,779	8>
USGS-9	654492	258101	5,032	9	5,000	0	4,878	38	—	0
USGS-86	667053	243371	5,081	14	—	0	—	0	—	0
USGS-87	670635	266881	5,016	3	4,975	5	4,920	0	4,787	15
USGS-88	667356	265453	5,020	5	5,015	0	4,917	11	4,789	33
USGS-89	669957	263286	5,029	10	4,985	0	4,932	14	4,798	14
USGS-90	668552	269602	5,010	5	5,005	0	4,906	22	4,763	5
USGS-91	669100	268150	5,006	9	4,997	0	4,910	15	4,777	19
USGS-92	669408	266121	5,008	19	4,989	0	4,922	5	4,790	28
USGS-93	669566	265067	5,010	13	4,997	0	4,914	12	4,792	11
USGS-93A	669566	265179	5,010	11	4,999	0	4,916	13	4,793	9
USGS-94	669150	266050	5,008	12	4,996	0	4,915	18	4,788	26
USGS-95	668770	267038	5,008	23	4,985	0	4,912	16	4,786	12
USGS-96	669750	265700	5,009	13	4,978	4	4,912	27	4,790	10
USGS-96B	669754	265337	5,009	14	4,977	5	4,911	28	4,791	11>
USGS-105	651355	277395	5,090	15	5,075	0	—	0	—	0
USGS-106	669059	280994	5,017	3	5,014	0	4,886	22	—	0
USGS-108	650807	285611	5,033	7	5,026	0	4,844	82	4,715	0
USGS-109	651255	265736	5,045	1	5,044	0	4,873	12	—	0
USGS-117	668800	265711	5,012	14	4,998	0	4,915	5	4,789	28

Table 5-9. **(continued).**

Common Well Name	Northing (ft)	Easting (ft)	Surface Elevation (ft amsl)	Thickness (ft)	A-B Interbed Elevation (ft amsl)	Thickness (ft)	B-C Interbed Elevation (ft amsl)	Thickness (ft)	C-D Interbed Elevation (ft amsl)	Thickness (ft)
USGS-118	668007	267802	5,013	14	4,999	0	4,910	11	4,791	28
USGS-119	667780	267541	5,031	3	5,028	0	4,919	5	4,783	19
USGS-120	665237	264542	5,042	12	5,030	0	4,911	40	4,790	14
DO-2	669683	267180	5,012	15	4,984	3	4,914	5	4,789	12>
DO-6	669806	266863	5,012	3	4,973	9	4,925	0	—	—
DO-6A	669796	266860	5,012	2	4,971	9>	—	—	—	—
D-10	669739	265331	5,009	9	4,981	9	4,916	2	4,791	11
D-15	668966	264930	5,011	2	4,980	4	4,917	18	4,793	20
RWMC	669659	269011	5,005	7	4,998	0	4,909	6	4,786	17
TW-1	669689	267177	5,010	14	4,977	0	4,913	5	4,789	17>
Test Well	665238	264743	5,042	3	5,039	0	4,912	10	4,788	20
WWW#1	669941	263210	5,036	5	4,992	11	4,931	16	4,805	21
WWW#2	669689	263116	5,036	3	5,001	10	4,933	18>	—	—
VZT-1	670702	266975	5,018	4	4,975	7	4,918	18	—	—
C-1	671675	269780	5,029	2	4,993	2	4,909	5	4,799	10
C-1A	671707	269792	5,029	4	4,993	0	4,911	4	4,799	12
Rif-Ran	685752	282883	4,967	9	4,958	20	4,849	0	4,821	0
HWY-3	687065	277159	4,981	21	4,960	14	4,835	0	4,816	0
EBR-I	674268	276993	5,024	11	5,013	0	4,900	24	4,788	5
A11A31	662517	268728	5,065	3	5,062	0	4,892	66	4,782	35
0W-1	665336	264794	5,042	5	5,037	0	4,915	30	4,787	**14**

Table 5-9. (continued).

Common Well Name	Northing (ft)	Easting (ft)	Surface Elevation (ft amsl)	Thickness (ft)	A-B Interbed Elevation (ft amsl)	Thickness (ft)	B-C Interbed Elevation (ft amsl)	Thickness (ft)	C-D Interbed Elevation (ft amsl)	Thickness (ft)
ow-2	664910	264932	5,044	7	5,037	0	4,910	42	4,784	4
NA89-1	669083	259758	5,045	2	4,995	0	4,931	17	4,821	8
NA89-2	675154	257588	5,059	12	5,014	0	4,863	4	—	—
NA89-3	665178	264344	5,038	1	5,037	0	4,909	4,6	—	—
M1SA	668992	264962	5,011	7	4,980	5	4,917	20	4,790	20
M3S	670165	268700	5,016	5	4,989	3	4,910	15	4,792	3
M4D	667255	265510	5,023	8	5,015	0	4,914	29	4,787	28
M6S	666379	270722	5,066	7	5,059	0	4,900	10	4,74,6	18
M7S	671588	270921	5,005	9	4,996	0	4,908	6	4,782	0
M10S	668227	266882	5,022	6	5,016	0	4,910	24	4,789	27
VVE-1	669009	264964	5,011	8	4,980	6	4,917	22	4,792	23>
VVE-3	670163	268676	5,015	6	4,987	4	4,909	14	4,792	10>
VVE-4	667253	265486	5,022	8	5,000	15	4,916	31	4,787	23>
VVE-6A	666368	270684	5,066	4	5,062	0	4,903	14	—	—
VVE-7	671608	270919	5,004	14	4,990	0	4,887	11	4,784	7>
VVE-10	668241	266869	5,021	6	5,015	0	4,908	24	4,781	18>
1E	669475	268396	5,006	15	4,991	0	4,907	7>	—	—
1V	669619	268429	5,006	9	4,997	0	4,911	7	—	—
2E	669438	267553	5,008	15	4,979	3	4,912	3>	—	—
2v	668845	268259	5,006	7	4,999	0	4,910	9	4,767	3>
3E	669775	267147	5,012	5	5,007	0	4,913	3	—	—

Table 5-9. (continued).

Common Well Name	Northing (ft)	Easting (ft)	Surface Elevation (ft amsl)	Thickness (ft)	A-B Interbed Elevation (ft amsl)	Thickness (ft)	B-C Interbed Elevation (ft amsl)	Thickness (ft)	C-D Interbed Elevation (ft amsl)	Thickness (ft)
3v	669690	267564	5,009	17	4,982	4	4,910	4	4,787	2>
4E	669265	266600	5,014	23	4,991	0	4,913	4>	—	—
4v	668980	267320	5,012	10	5,002	0	4,908	13	4,781	4>
5E	669403	265750	5,013	21	4,992	0	4,916	4>	—	—
5v	668885	266555	5,011	9	4,992	7	4,913	3	—	—
6V	669688	266352	5,017	10	4,986	7	4,926	4	4,793	2>
7v	669370	266113	5,009	15	4,987	7	4,925	10	4,786	5>
8V	669190	265723	5,012	21	4,991	0	4,914	37	4,786	1>
9v	669845	265754	5,014	20	4,994	0	4,913	20	4,786	I>
10V	669572	265022	5,013	10	4,993	9	4,916	14	4,789	5>
M11S	675132	274247	4,994	10	4,984	0	4,903	5	4,787	23
M12S	677145	280877	4,975	8	4,967	0	4,911	2	4,783	12
M13S	672953	276945	5,027	16	5,011	0	4,894	12	4,781	0
M14S	674610	266413	5,032	7	5,025	0	4,904	0	4,824	0
M15S	668207	271193	5,019	18	5,001	0	4,889	27	4,789	15
M16S	670185	271201	5,004	18	4,986	0	4,886	10	4,807	12
M17S	669364	267183	5,012	23	4,989	0	4,911	10	4,784	22
I-1S	669563	264936	5,013	8	5,005	0	4,913	11	—	—
I-ID	669563	265041	—	—	—	—	—	—	4,790	20
1-2s	669413	265632	5,014	18	4,996	0	4,911	11	—	—
I-2D	669427	265396	—	—	—	—	—	—	4.791	1

Table 5-9. (continued).

Common Well Name	Northing (ft)	Easting (ft)	Surface Elevation (ft amsl)	Thickness (ft)	A-B Interbed Elevation (ft amsl)	Thickness (ft)	B-C Interbed Elevation (ft amsl)	Thickness (ft)	C-D Interbed Elevation (ft amsl)	Thickness (ft)
I-3S	669406	266280	5,012	16	4,985	2	4,914	4	—	—
I-3D	669405	266304	—	—	—	—	—	—	4,787	11>
I-4S	669462	266907	5,009	15	4,994	0	4,912	2	—	—
I-4D	669462	266932	—	—	—	—	—	—	4,787	16>
I-5S	669366	267132	5,012	32	4,980	0	4,913	6>	—	—
O-1	669140	264952	5,011	8	4,979	1	4,917	18	4,790	15>
0-2	668242	267356	5,014	5	5,009	0	4,907	18	4,771	7
0-3	670011	266496	5,010	8	4,975	9	4,919	12	4,789	15>
0-4	669607	264543	5,014	11	4,970	7	4,909	18	4,789	19>
0-5	669423	263931	5,021	2	4,976	6	4,916	23	4,789	26
0-6	668606	264939	5,013	10	4,982	6	4,905	14	4,789	26>
0-7	667762	264503	5,033	4	5,006	6	4,915	34	4,788	4>
0-8	668715	268351	5,010	8	5,002	0	4,910	0	4,777	1>

amsl (above mean sea level)

- indicates that either the interbed was absent or lithologic information could not be extracted from the data.

> indicates partial penetration of an interbed.

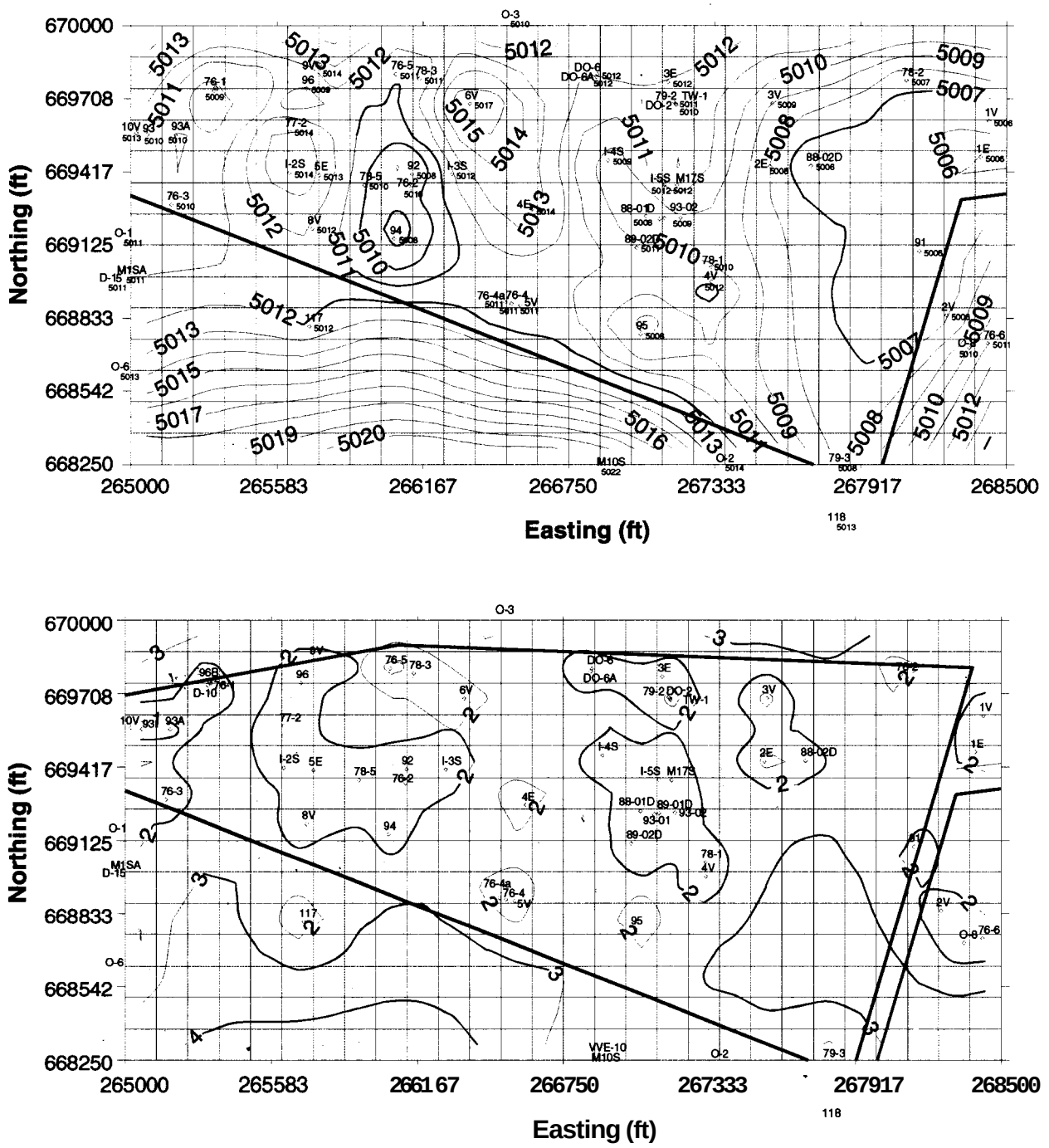

Figure 5-5. The top plot shows the final kriged results for elevations (ft amsl) of surficial sediments for the second level of grid refinement. The bottom plot shows uncertainty (standard error) in the elevations of surficial sediments for the same grid.

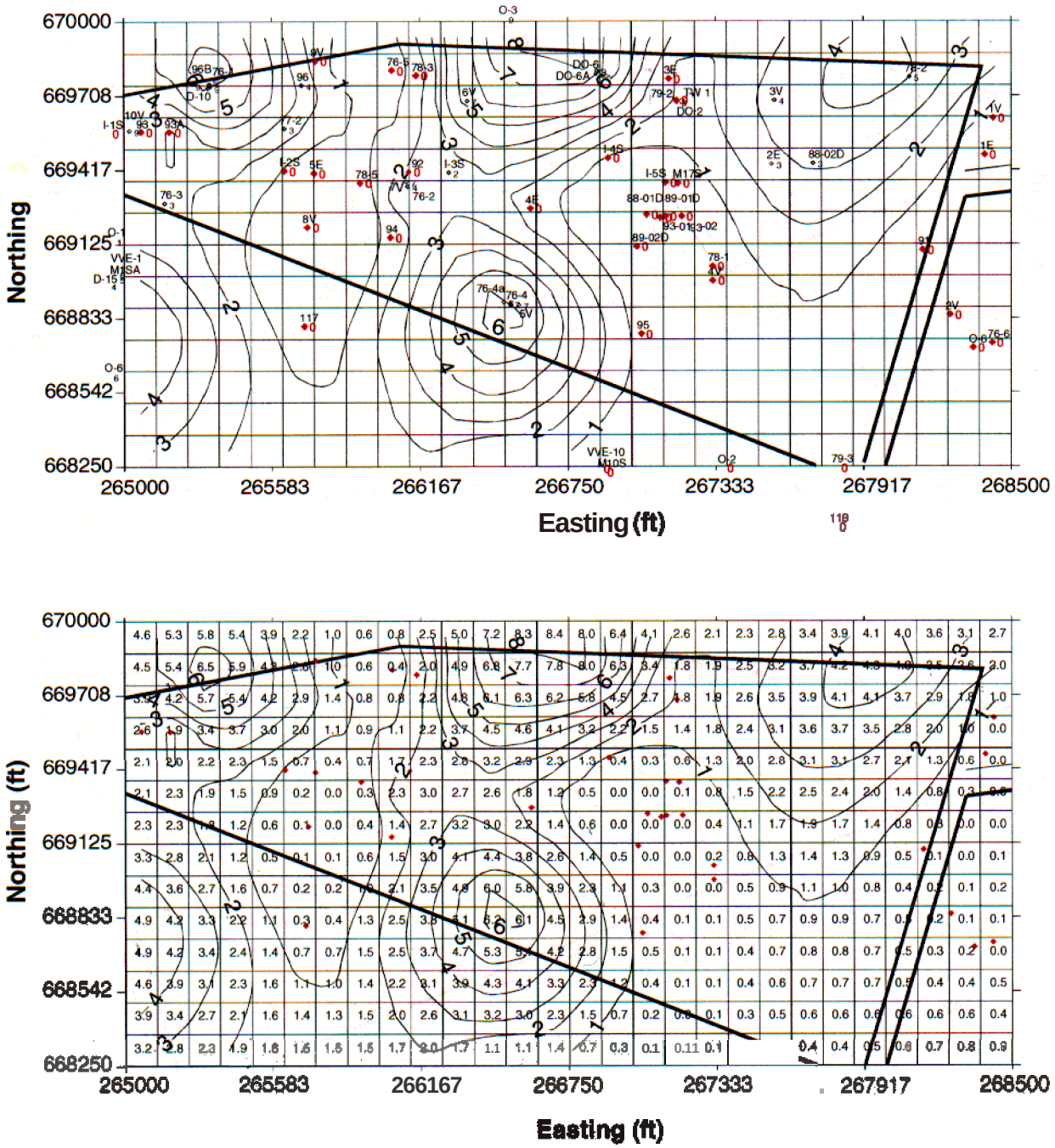

Figure 5-6. Kriged results for the A-B interbed thickness (ft) on the second level of grid refinement. Colored markers indicate locations of zero thickness. The lower plot has only colored markers for zero thickness locations and the matrix of kriging results are superimposed. Note the persistence of locations with zero thickness into the kriging results.

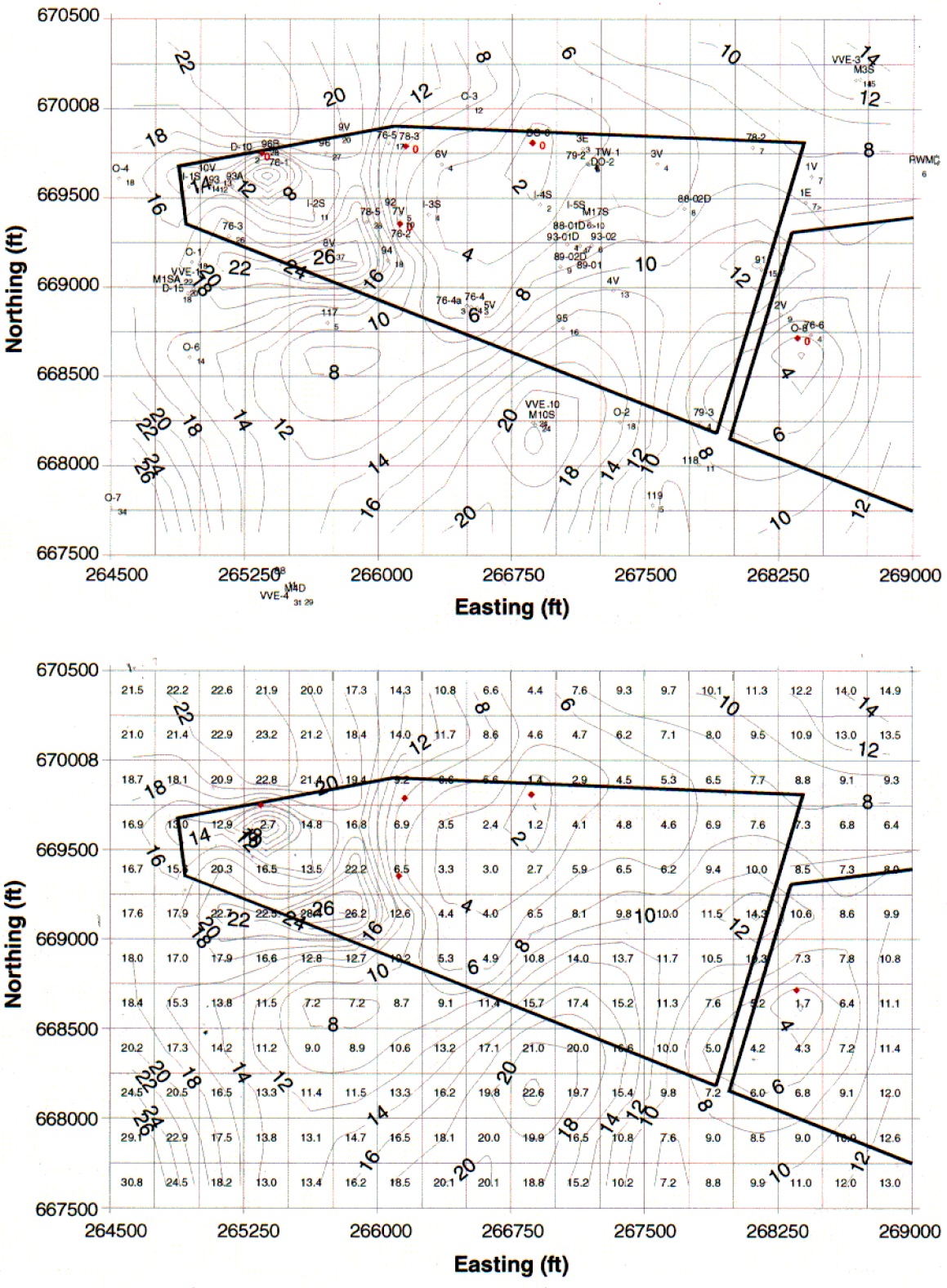

Figure 5-7. Kriged results for the B-C interbed thickness (ft) on the first level of grid refinement. Colored markers indicate locations of zero thickness. The lower plot has only colored markers for zero thickness locations and the matrix of kriging results are superimposed. Note the lack of persistence of locations with zero thickness into kriging results.

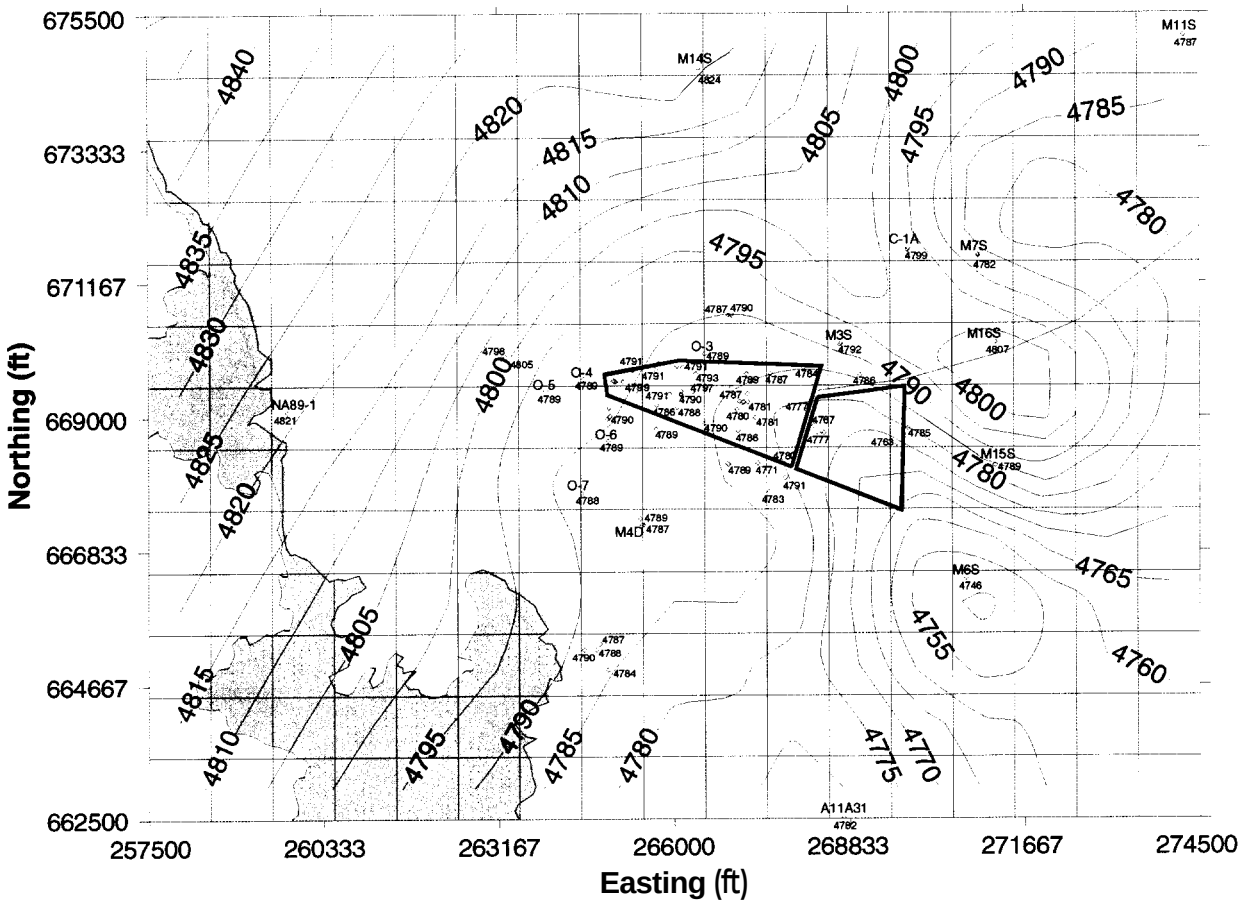

Figure **5-8.** Kriged results for the elevation of the top surface of the C-D interbed for the initial vadose zone base grid. Note an interpolated saddle feature between Wells **M3S** and **M7S** and a trough feature leading southeasterly from the Subsurface Disposal Area toward Well **M6S**.

Table **5-10.** Variogram parameters used in universal kriging of elevations and interbed soil thickness.

Variable	Nugget[a] (ft^2)	Sill[a] (ft^2)	Range (ft)	Interpolation Method
Surface elevation	0	**25**	**1,300**	Universal kriging
Surficial soil thickness	**5**	**44**	**600**	Simple kriging
A basalt elevation	0	**170**	1,800	Simple kriging
Thickness of the A-B interbed soil	**1**	**4**	**850**	Universal kriging
B basalt elevation	**5**	31	2,900	Universal kriging
Thickness of the B-C interbed soil	0	120	3,000	Simple kriging
C basalt elevation	0	**45**	2,200	Universal kriging
Thickness of the C-D interbed soil	**40**	**50**	**700**	Universal kriging

a. Nuggets and sills are fitting parameters that describe irreducible local variance and overall population variance (Leecaster 2002).

The last plot in this sequence (see Figure 5-8) shows kriging results for the elevation of the top of the C-D interbed for the initial vadose zone domain. Though this domain was not used in the simulations contained in this report, the figure is included because of the interesting feature near Well M7S to the northeast of the SDA. A saddle feature in the upper surface of the C-D interbed was interpolated between Wells M7S and M3S. This topologic feature, if it really exists at the SDA, may enhance the movement of contaminants that move in the vapor phase after they are present in sufficient concentrations to begin diffusing or advecting in the gaseous phase over the saddle, thus aiding the movement of such contaminants in a northeasterly direction from the SDA. Also visible in this plot is a trough feature or depression leading southeasterly from the SDA toward Well M6S. Elevated concentrations of chromium and nitrate in Well M6S (discussed in Sections 5.2.4.6) may result from preferential migration aided by the presence of this trough.

5.2.4.3.3 Vertical Conformable *Gridding*—The next step in development of the ABRA vadose zone model was vertical discretization of the base simulation domain. The kriged lithologic surfaces were used in conjunction with the horizontally discretized domains to create a conformable vertical grid. Minimum vertical grid size, maximum vertical grid size, and a geometric factor for increasing vertically adjacent grid blocks were assigned a priori for each lithologic unit in the base vadose zone domain. Minimum grid size was 0.5 m (1.6 ft) for each of the sediment and basalt units, except for the A-B interbed where a minimum grid size of 0.4 m (1 ft) was assigned. The geometric factor for the ratio between successive vertical grid blocks was a maximum of 1.5, which is a commonly used ratio to ensure numerical accuracy. Maximum vertical grid block size was 3 m (9.8 ft) in the sediment units and 10 m (33 ft) in the basalts. Logic for adjusting vertical grid block sizes was applied vertically at each horizontal grid block location to allow for an optimum match of the grid block interfaces to the kriged surface elevations. By having the same minimum grid block size specified for both sediment features and basalt features, uniformity of grid block sizes was ensured across lithologic interfaces. The total number of vertical grid blocks was determined through this process and resulted in 72 vertical grid blocks at each horizontal location for the base vadose zone simulation domain. The upper surface of the vadose zone simulation domain was variable and was determined from the kriged elevation for the surficial sediments. The lower surface of the vadose zone simulation domain was arbitrarily assigned as a flat plane. The lowest level of the vadose zone simulation domain was inadvertently assigned an elevation that was actually 27.5 m (90 ft) above the aquifer. This truncated vadose zone domain resulted in slightly decreased water and contaminant travel times through the vadose zone domain because water and contaminant movement in the fractured basalt portion were assigned values to make water movement very fast. Also, there was no intention to include interbeds in this lowest 27.5 m (90 ft). Therefore, the truncation of the vadose zone domain and slight decrease in water and contaminant travel times through the vadose zone domain was insignificant.

The logic for vertical grid discretization was different for the refined areas. Vertical discretization for the base domain was not further adjusted based on the kriged elevations in the refined grids. Rather, the kriged elevations for the refined grids were compared to the conformable vertical discretization determined from the base grid and then, as necessary, the material properties assigned in the refined domains were adjusted. This process resulted in smooth-appearing grid interfaces in the base domain and some degree of stair-stepping in the refined grids. This can be seen in Figures 5-9, 5-10, and 5-11, which show three-dimensional views of the resulting grids starting with the base grid and ending with the second-level grid refinement. These three-dimensional views are distorted both horizontally and vertically because the software (Visual Numerics 1996) that produces them projects onto a cube. The outline of the SDA is shown in each case projected just above the cube. The vertical extent shown in each figure is indicated in the captions.

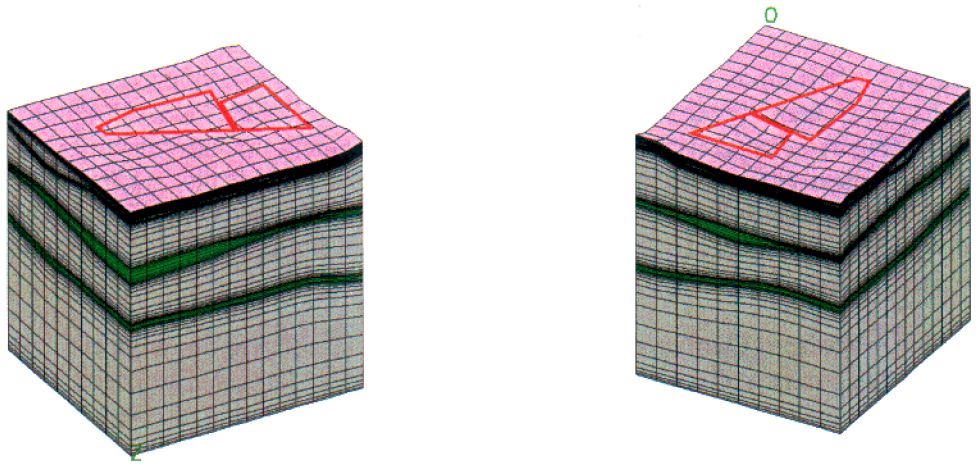

Figure 5-9. Southwest and northeast views of base grid beneath the Subsurface Disposal Area showing vertical conformable gridding. The vertical extent shows the entire vadose zone simulation domain. Interbed grids are shaded green and fractured basalt grids are shaded gray.

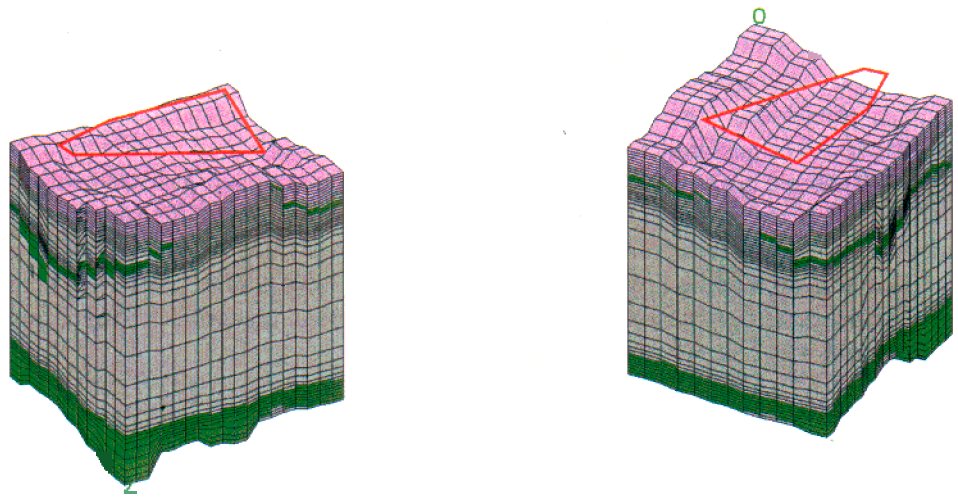

Figure 5-10. Southwest and northeast views of first-level refined grid showing vertical conformable gridding. The first level of grid refinement extended to the base of the B-C interbed beneath the Subsurface Disposal Area.

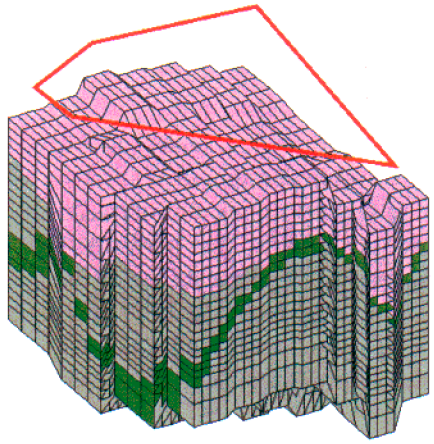

Figure 5-11. Southwest view of the second-level refined grid showing vertical conformable gridding. The second level of grid refinement extended to the base of the A-B interbed beneath the Subsurface Disposal Area. Note the A-B interbed merging with the surficial sediments.

5.2.4.3.4 Hydrologic Property Assignment —Hydrologic properties for porosity and permeability for the surficial sediments, the A-B interbed, and the fractured basalt were assigned the same properties as the IRA model (see Table 5-11) because no new information was available for these units.

Table 5-11. Parameterization of hydrologic properties and source of parameters for surficial sediments, A-B interbed, and fractured basalt.

Parameter	Permeability	Porosity
Surficial sediments	680 milliDarcy (mD), isotropic. Average of calibrated properties in Martian (1995).	0.50 cm^3/cm^3 (Martian 1995)
A-B interbed	4 mD. Waste Area Group 3 modeling in Rodriguez et al. (1997).	0.57 cm^3/cm^3 (Magnuson and McElroy 1993)
Fractured basalt	300 mD vertical and 9,000 mD horizontal in Magnuson (1995).	0.05 cm^3/cm^3 (Magnuson 1995)

The moisture characteristic curve (also known as the water release curve or theta-psi curve) for all of the sediment features was based on the empirical relationship determined by van Genuchten (1980). The parameters assigned for the van Genuchten curve were taken from the GWSCREEN (Rood 1999) default values that were based on the average of four SDA surficial sediment samples that were hydraulically characterized and reported in Baca et al. (1992). The values for residual moisture content, van Genuchten alpha, and van Genuchten N were 0.142 cm^3/cm^3, 1.066 m^{-1}, and 1.523 (dimensionless), respectively. This was a slightly different approach from that used in the IRA model and was used to obtain numerical convergence. The moisture characteristic curves used in the IRA model were tested with the new conformable grid; however, a stable solution could not be obtained.

The moisture characteristic curve used for the fractured basalts was the same as that used for the IRA model. Sensitivity simulations performed to investigate the appropriateness of this moisture characteristic curve are discussed below.

A major difference between the IRA model and the model used to make the simulations presented in this report was the use of spatially variable permeabilities and porosities for the B-C and C-D interbeds. The spatial variability analyses used to krige porosity and permeability onto the simulation grids are contained in Leecaster **(2002).** A process similar to that performed for the lithology analysis (discussed above) was also performed for the porosity and permeability of the B-C and C-D interbeds. The data set consisted of **112** samples, the majority coming from the **1999** drilling activities. Scale issues associated with using core sample results applied to much larger areas are acknowledged but not addressed in this modeling exercise. These **112** samples represented **32** site locations, **17** in the B-C interbed and **24** in the C-D interbed. Some of the sites were for the same well. The porosity data from multiple depths across an individual interbed were arithmetically averaged. Likewise, the permeability data were combined by harmonic averaging because the primary flow direction was interpreted to be vertical across the layers, Figures **5-12** and **5-13** show the kriged porosity and permeabilities for the B-C and C-D interbeds, respectively. Only the most refined grid for each interbed is shown, which is the base grid for the C-D interbed and the first level of grid refinement for the B-C interbed. Standard errors for the kriging results are presented in Leecaster **(2002).**

Similar to the IRA model, a low permeability of 1 milliDarcy (mD) and a low porosity of 0.05 were assigned to the top grid block representing both the B-C and C-D interbeds. This was accomplished by identifying the uppermost grid block representing each interbed in the grid with the greatest level of refinement, and then assigning the low porosity and low permeability value to that grid block. This low permeability feature is considered representative of either a low permeability sedimentary feature at the top of the interbeds or a low permeability feature caused by fine sediments infilling fractures in the basalts immediately above the interbed. Inclusion of this low permeability, low porosity feature was necessary to create conditions close to saturation at locations within the interbeds and to facilitate spreading of water from where it was applied at depth above the C-D interbed to include the effect of spreading-area water. The latter topic is discussed below.

5.2.4.3.5 Boundary and Initial Conditions — Boundary conditions for the vadose zone model primarily consist of assigning surface water fluxes. Two types of water fluxes were imposed on the simulation domain representing steady-state conditions and historical flooding conditions. No additional information existed by which to assign background infiltration inside the SDA; therefore, the fluxes were assigned in a manner to mimic the infiltration pattern of the IRA model as close as possible with a constraint to maintain an overall average of 8.5 cm/year **(3.3** in./year) inside the SDA (see Figure **5-14).** The same low, medium, and high infiltration rates of 0.64 cm/year **(0.25** in./year), **3.68** cm/year **(1.45** in./year), and **24.1** cm/year **(9.48** in./year) from the IRA model were used. The original assignment in the IRA model was based on interpretations of neutron moisture monitoring and surface topography made in Martian **(1995).** Outside the SDA, surface infiltration was assigned the same rate of 1 cm/year **(0.4** in./year) based on Cecil et al **(1992).**